



UNIVERSIDAD DE INVESTIGACIÓN DE TECNOLOGÍA EXPERIMENTAL YACHAY

Escuela de Ciencias Físicas y Nanotecnología

**TÍTULO: Study of dense molecular gas in three local galaxies with
data from the Gran Telescopio Milimétrico “Alfonso Serrano”**

Trabajo de integración curricular presentado como requisito para la
obtención del título de Físico

Autor:

Ñauñay Chicaiza Jéssica Pamela

Tutor:

Ph. D. Ramirez Velasquez José Manuel

Co - Tutor:

Ph. D. Vega Casanova Olga Mercedes

Urcuquí, Febrero 2021

SECRETARÍA GENERAL
(Vicerrectorado Académico/Cancillería)
ESCUELA DE CIENCIAS FÍSICAS Y NANOTECNOLOGÍA
CARRERA DE FÍSICA
ACTA DE DEFENSA No. UITEY-PHY-2020-00028-AD

En la ciudad de San Miguel de Urcuquí, Provincia de Imbabura, a los 18 días del mes de diciembre de 2020, a las 12:00 horas, en el Aula CHA-01 de la Universidad de Investigación de Tecnología Experimental Yachay y ante el Tribunal Calificador, integrado por los docentes:

Presidente Tribunal de Defensa	Dra. ROJAS CELY CLARA INES , Ph.D.
Miembro No Tutor	Dr. YEPES RAMIREZ, HAROLD , Ph.D.
Tutor	Dr. RAMÍREZ JOSÉ MANUEL , Ph.D.

Se presenta el(la) señor(ita) estudiante **ÑAUÑAY CHICAIZA, JESSICA PAMELA**, con cédula de identidad No. **1720212768**, de la **ESCUELA DE CIENCIAS FÍSICAS Y NANOTECNOLOGÍA**, de la Carrera de **FÍSICA**, aprobada por el Consejo de Educación Superior (CES), mediante Resolución **RPC-SO-39-No.456-2014**, con el objeto de rendir la sustentación de su trabajo de titulación denominado: **STUDY OF DENSE MOLECULAR GAS IN THREE LOCAL GALAXIES WITH DATA FROM THE GRAN TELESCOPIO MILIMÉTRICO**, previa a la obtención del título de **FÍSICO/A**.

El citado trabajo de titulación, fue debidamente aprobado por el(los) docente(s):

Tutor	Dr. RAMÍREZ JOSÉ MANUEL , Ph.D.
--------------	---------------------------------

Y recibió las observaciones de los otros miembros del Tribunal Calificador, las mismas que han sido incorporadas por el(la) estudiante.

Previamente cumplidos los requisitos legales y reglamentarios, el trabajo de titulación fue sustentado por el(la) estudiante y examinado por los miembros del Tribunal Calificador. Escuchada la sustentación del trabajo de titulación, que integró la exposición de el(la) estudiante sobre el contenido de la misma y las preguntas formuladas por los miembros del Tribunal, se califica la sustentación del trabajo de titulación con las siguientes calificaciones:

Tipo	Docente	Calificación
Tutor	Dr. RAMÍREZ JOSÉ MANUEL , Ph.D.	9,8
Presidente Tribunal De Defensa	Dra. ROJAS CELY CLARA INES , Ph.D.	9,6
Miembro Tribunal De Defensa	Dr. YEPES RAMIREZ, HAROLD , Ph.D.	8,6

Lo que da un promedio de: **9.3 (Nueve punto Tres)**, sobre 10 (diez), equivalente a: **APROBADO**

Para constancia de lo actuado, firman los miembros del Tribunal Calificador, el/la estudiante y el/la secretario ad-hoc.

ÑAUÑAY CHICAIZA, JESSICA PAMELA
Estudiante

Dra. ROJAS CELY CLARA INES , Ph.D.
Presidente Tribunal de Defensa

CLARA
 INES ROJAS
 CELY
 Digitally signed
 by CLARA INES
 ROJAS CELY
 Date: 2021.01.08
 11:27:56 -05'00'

Dr. RAMÍREZ JOSÉ MANUEL , Ph.D.
Tutor

JOSE MANUEL
 RAMIREZ
 VELASQUEZ
 Digitally signed by
 JOSE MANUEL
 RAMIREZ VELASQUEZ
 Date: 2021.01.08
 14:58:57 -05'00'

Dr. YEPES RAMIREZ, HAROLD , Ph.D.
Miembro No Tutor

CARLA SOFIA
YASELGA NARANJO

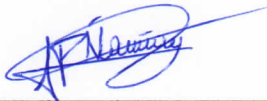
Digitally signed by CARLA SOFIA
YASELGA NARANJO
Date: 2021.01.08 10:46:52 -05'00'

YASELGA NARANJO, CARLA
Secretario Ad-hoc

AUTORÍA

Yo, **JÉSSICA PAMELA ÑAÑAY CHICAIZA**, con cédula de identidad 1720212768, declaro que las ideas, juicios, valoraciones, interpretaciones, consultas bibliográficas, definiciones y conceptualizaciones expuestas en el presente trabajo; así como, los procedimientos y herramientas utilizadas en la investigación, son de absoluta responsabilidad de el/la autora (a) del trabajo de integración curricular. Así mismo, me acojo a los reglamentos internos de la Universidad de Investigación de Tecnología Experimental Yachay.

Urququí, febrero 2021.




Jéssica Pamela Ñañay Chicaiza
CI: 1720212768

AUTORIZACIÓN DE PUBLICACIÓN

Yo, **JÉSSICA PAMELA ÑAÑAY CHICAIZA**, con cédula de identidad 1720212768, cedo a la Universidad de Tecnología Experimental Yachay, los derechos de publicación de la presente obra, sin que deba haber un reconocimiento económico por este concepto. Declaro además que el texto del presente trabajo de titulación no podrá ser cedido a ninguna empresa editorial para su publicación u otros fines, sin contar previamente con la autorización escrita de la Universidad.

Asimismo, autorizo a la Universidad que realice la digitalización y publicación de este trabajo de integración curricular en el repositorio virtual, de conformidad a lo dispuesto en el Art. 144 de la Ley Orgánica de Educación Superior

Urcuquí, febrero 2021.



Jéssica Pamela Ñañay Chicaiza
CI: 1720212768

Acknowledgements

In this section I want to express my sincere thanks to those people who in one way or another contributed and supported me on the development this work, and with the end of an important stage in my life.

First of all, I want to thank my advisor and co-advisor. Ph. D. José Ramirez, my advisor, thank you for sharing your knowledge and for guiding me for the good completion of this thesis. Ph. D. Olga Vega, my co-advisor, who from the first moment I mentioned that I would like to work with her, showed total predisposition. This positive and enthusiastic attitude was evident throughout the development of this work. She knew how to guide me and explain me patiently, and, above all, she knew how to make me feel confident about my abilities. In the same way, I want to thank INAOE for giving me the opportunity to have contact with this wonderful science that I am passionate about as astrophysics.

A special thanks to all the professors who are part of the School of Physical Sciences and Nanotechnology of Yachay Tech University who during the last three years of my life have shared their knowledge with me, have guided and encouraged me in a way that I can improve myself every day, and who have been an inspiration for me. About the last aspect, I want to mention professors Clara Rojas and Mayra Peralta who are women scientists that with sacrifice and effort have achieved great things, my sincere admiration for you.

On the other hand, apart from the academic field, I want to thank all my family who have been my support during this great trajectory. I especially want to thank my parents, Mónica and Leopoldo, who have sacrificed many things so that I could obtain the best education, and the results of all that sacrifice are reflected in the development of this work. Everything that I have achieved is by and for you, and do not doubt that I will always give my best to make you feel proud of me.

Last but not least, I want to thank all my friends and classmates with whom I have shared so many special moments. Patty, Jhoa, Eve, and Thaly, you are strong women who inspire me, thank you very much for sharing so many laughs, and being great and true friends for me. Antho and Oscar you are friends who have been able to listen and advise me, and for that I am very grateful to you. Andy, Fabi and Iskra, my study partners and great friends, with you I have spent the hardest stages of my university life, so many sleepless nights, so many hours studying together and explaining topics to each other, all this has been worth the pain. We did it my friends.

This achievement would not have been possible without the participation and support of you, my biggest and most sincere thanks to all of you.

Jéssica Pamela Ñauñay Chicaiza

Resumen

En este trabajo, he analizado los espectros moleculares en la banda de los 3 mm de tres galaxias locales, dos Núcleos Galácticos Activos (AGN) como NGC 4826 y NGC 4414, y una galaxia tipo Starburst como NGC 2903. Los datos fueron tomados con Redshift Search Receiver (RSR) del Gran Telescopio Milimétrico (LMT) de 32 m en el rango de frecuencia $\sim [73 - 111]$ GHz. Este trabajo busca identificar moléculas características de los AGN y / o galaxias tipo Starburst. Primero, he identificado las especies moleculares en cada galaxia, encontrando veintitrés especies moleculares en NGC 4826, veintiocho en NGC 2903 y nueve en NGC 4414. Luego, calculé la intensidad de la línea molecular de las especies moleculares identificadas más relevantes usando un ajuste gaussiano. Luego, asumiendo Equilibrio Termodinámico Local (LTE) con una temperatura de 10 K, calculé las densidades columnales de estas especies moleculares. Se realizó una estimación del límite superior para aquellas moléculas que no se identificaron en las tres galaxias de mi muestra. Se estimaron brevemente algunos parámetros físicos del medio molecular utilizando los isótopos de ^{13}CO y C^{18}O identificados en mis tres galaxias. Finalmente, los resultados obtenidos se compararon con la literatura para saber si las galaxias estudiadas en este trabajo tenían comportamientos típicos de galaxias cuya actividad nuclear era similar. Esta comparación se realizó tanto visual como empíricamente.

Keywords:

NGC 4826, NGC 2903, NGC 4414, IM:cloud, IM:abundances.

Abstract

In this work, I have analyzed the molecular spectra in the 3 mm band towards three local galaxies, two Active Galactic Nucleus (AGN) like NGC 4826 and NGC 4414, and one Starburst type galaxy like NGC 2903. The data were taken with the Redshift Search Receiver (RSR) of the 32 m Large Millimeter Telescope (LMT) in the frequency range $\sim [73 - 111]$ GHz. This work seeks to identify molecules that are characteristic of AGNs and/or Starburst type galaxies. First, I identify the molecular species in each galaxy, finding twenty three molecular species in NGC 4826, twenty eight in NGC 2903, and nine in NGC 4414. Next, I calculated the molecular line intensity of the most relevant identified molecular species by using a Gaussian fitting. Then, assuming Local Thermodynamic Equilibrium (LTE) with a temperature of 10 K, I estimated the column densities of these molecular species. An upper limit estimation was performed for those molecules that were not identified in the three galaxies of my sample. Some physical parameters of the molecular medium were briefly estimated by using the ^{13}CO and C^{18}O isotopes identified in my three galaxies. Finally, the obtained results were compared with the literature to know if the galaxies studied on this work had typical behaviors of galaxies whose nuclear activity was similar. This comparison was made both visually and empirically.

Keywords:

NGC 4826, NGC 2903, NGC 4414, IM:cloud, IM:abundances.

Contents

List of Figures	viii
List of Tables	x
1 Introduction	1
1.1 Galaxies	1
1.2 Star formation, nuclear activity, and molecular gas	6
1.2.1 Definition of star formation	6
1.2.2 Molecular clouds and their connection with star formation	6
1.2.3 Local Thermodynamic Equilibrium	8
1.2.4 Molecular emission	9
1.2.5 Dense gas tracer molecules	9
1.3 Problem Statement	11
1.4 General and Specific Objectives	12
1.4.1 General Objective	12
1.4.2 Specific Objectives	12
2 Methodology	13
2.1 The sample of the galaxies	13
2.1.1 NGC 4826	13
2.1.2 NGC 2903	14
2.1.3 NGC 4414	14
2.2 Description of the telescope (LTM)	15
2.2.1 Antenna	16
2.2.2 Instrumentation	16
2.3 Observations and data reduction	18
2.3.1 Observations	18
2.3.2 Data reduction	19

3	Results	21
3.1	Molecular Lines Identification	21
3.2	Molecular Line Intensities Calculation	23
3.3	Column Densities Estimation	31
3.4	Estimation of physical parameters of the molecular medium in my galaxies	33
3.4.1	Excitation Temperature	34
3.4.2	Optical Depth	34
3.4.3	H_2 Column Density	35
4	Analysis & Discussion of Results	37
4.1	Comparison between the spectra of the galaxies	37
4.1.1	Line Ratios	40
4.2	Comparison between the abundances of the galaxies	41
4.2.1	Molecules	41
4.2.2	Abundance Ratios	44
5	Conclusions	49
5.1	Conclusions	49
5.2	Future Research	50
A	Errors Propagation	53
	Bibliography	55
	Abbreviations	61

List of Figures

1.1	“The Sequence of Nebular Types” diagram published by Edwin Hubble in 1936 ¹	2
1.2	Hubble sequence of galaxies modified ²	2
1.3	Examples of elliptical galaxies.	3
1.4	Examples of spiral galaxies.	3
1.5	Examples of barred spiral galaxies.	4
1.6	Example of irregular galaxy	4
1.7	Examples of galaxies whose orientation towards the observer varies (face-on and edge-on spiral galaxies).	5
1.8	Stages of the star formation proposed by Shu et al. ³ a) Formation of slowly rotating nuclei from molecular clouds. b) Formation of a central protostar and a disk due to gravitational instability. c) Creation of a bipolar flow due to the accretion of the material. d) End of material fall creating a new star with a circumstellar disk.	7
2.1	General map of Mexico showing the site of the Large Millimeter Telescope (LMT) which is located near the city of Puebla.	15
2.2	General scheme of the Large Millimeter Telescope (LMT).	17
2.3	Spectrum of the three galaxies after the reduction process.	20
3.1	calculation of the rms using CLASS.	22
3.2	NGC 4826 spectrum between 75 and 111 Ghz. All the detected species in the galaxy are indicated.	25
3.3	NGC 2903 spectrum between 75 and 111 Ghz. All the detected species in the galaxy are indicated.	25
3.4	NGC 4414 spectrum between 75 and 111 GHz. All the detected species in the galaxy are indicated.	26
3.5	Example of how CLASS package of GILDAS works.	26
4.1	Spectra of eight galaxies taken from Aladro et al. (2015) ⁴	38
4.2	Spectra of three galaxies between 75 and 111 GHz normalized with respect to the ¹³ CO molecule.	39
4.3	Spectra of three galaxies between 75 and 111 GHz normalized with respect to the HCN molecule.	40
4.4	Comparison between the column densities of the galaxies. Black arrows indicate upper limit abundance.	42
4.5	Comparison between the column densities of the galaxies normalized with respect to C ¹⁸ O abundance.	45

4.6	Comparison between the column densities of the galaxies normalized with respect to HCN abundance.	46
4.7	Plots of the fractional molecular abundances relative to $C^{18}O$. These results represent the abundance correlation between NGC 2903 with a typical Starburst galaxy. The red dashed lines represents equal abundances between the galaxies.	47
4.8	Plots of the fractional molecular abundances relative to $C^{18}O$. These results represent the abundance correlation between NGC 4414 and NGC 4826 with a typical AGN. The red dashed lines represents equal abundances between the galaxies.	48

List of Tables

1.1	List of detected molecules in the interstellar and circumstellar medium so far. The molecules in square brackets have a cyclic structure, and the others have a linear one ⁵	10
2.1	Galaxies Properties.	14
2.2	Main specifications of the LMT.	16
2.3	Observational Parameters.	18
2.4	Main beam efficiencies used in this work.	19
3.1	Overall rms of the three galaxies.	22
3.2	RMS values in intervals for each galaxy.	23
3.3	List of the molecular species identified in the three galaxies. <i>Yes</i> and - represent the detected and non-detected molecule respectively for each galaxy of my survey.	24
3.4	Selected σ value for each galaxy to calculate the upper limit of the area integral.	27
3.5	List of the molecular species identified in NGC 4826 with their respective line parameters.	28
3.6	List of the molecular species identified in NGC 2903 with their respective line parameters.	29
3.7	List of the molecular species identified in NGC 4414 with their respective line parameters.	30
3.8	Detected molecular transitions for my galaxies.	31
3.9	Total column densities calculated for the three galaxies NGC 4826, NGC 2903, NGC 4414.	33
3.10	Excitation Temperatures ($T_{ext}^{J=1 \rightarrow 0}$) of the ^{13}CO molecule of the three galaxies.	34
3.11	Detected molecular transitions for my galaxies.	35
3.12	Column density of H_2 calculated for the three galaxies.	36
4.1	Comparison between the integrated intensities obtained in this work with those found in the literature.	41

Chapter 1

Introduction

1.1 Galaxies

Due to historical reasons and the technology of that time, the first classification for galaxies was carried out at optical wavelengths and focused on relatively nearby galaxies. From 1781 to 1847, Sir William Herschel and his son, using large telescopes, searched the sky for objects that they called ‘white nebulae’, and they were able to identify that these objects in their center had different degrees of concentration and apparently were flat. In 1845, Willian Parson labeled some of these objects as ‘spirals’, and here the morphology of galaxies began to matter for their classification. The main classes of galaxies were identified by photographs. In astronomy, this technique became more important in the late nineteenth century. In 1924, Edwin Hubble developed a system for the classification of galaxies. This classification is even used until today with some slight refinements².

Hubble using a reflector telescope located at the Mount Wilson Observatory in California photographed numerous galaxies. Using these photographs, he classified or categorized the galaxies based on the shape they had as spiral, barred spiral, elliptical, irregular, and peculiar, and this system is known as the Hubble morphological sequence of galaxy types⁶. Figure 1.1 shows the original figure of the sequence of Nebular Types that was published by Edwin Hubble in 1936. As we can see from this figure, Hubble did not consider irregular galaxies within their “classification sequence” because they showed no evidence of rotational symmetry. On the other hand, he included an intermediate state between elliptical galaxies and spiral galaxies that he called “Type S0” or lenticular galaxies. In this way, the Hubble sequence was made up of four types of galaxies: elliptical (E), lenticular (S0), spiral (S or SB), and irregular (Irr)⁷.

It is important to mention that scientists at that time thought that the diagram proposed by Hubble showed the time evolution of galaxies. They believed that the first galaxies to be formed in the universe were elliptical galaxies, then they became elliptical galaxies, and their last phase was to be spiral galaxies. This is the reason that until today elliptical galaxies are called “early type galaxies”, and spiral galaxies “late type galaxies”⁷.

Figure 1.2 shows an updated version of the classification proposed by Edwin Hubble.

Some main characteristics that distinguish each type of galaxy together with their respective subclasses are

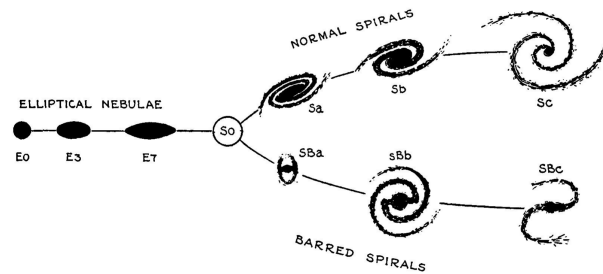


Figure 1.1: “The Sequence of Nebular Types” diagram published by Edwin Hubble in 1936¹.

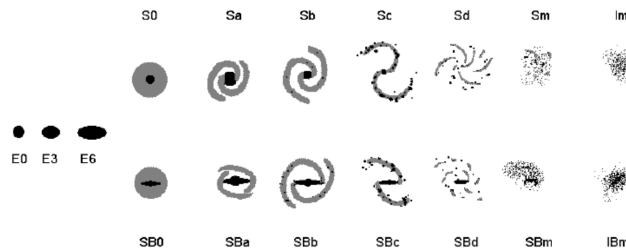


Figure 1.2: Hubble sequence of galaxies modified².

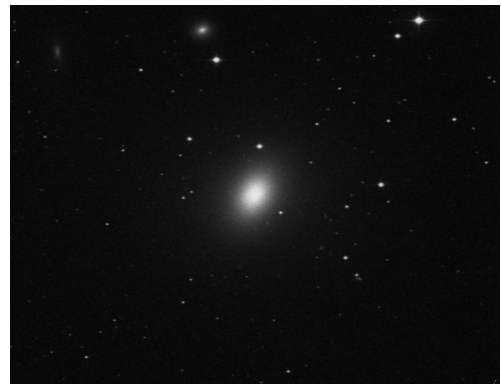
described below.

- **Elliptical Galaxies (E):** the criterion that Hubble used to classify this type of galaxy was its *ellipticity*. A numerical index n of ellipticity was added to the letter E: $n = 10(1 - b/a)$, where a and b are the major and minor axes of the ellipse that is formed in the sky plane by the projection of the galaxy. For instance, E0 galaxies are round or perfectly circular, while E6 galaxies are highly elongated or very flattened². Figure 1.3 shows two examples of elliptical galaxies: NGC 0221 or also known as Messier 32 (M32) classified as E2 galaxy, and NGC 462 (M59) classified as E5 galaxy. The images were obtained from “The STScI Digitized Sky Survey”ⁱ
- **Spiral Galaxies (S):** these types of galaxies are characterized by the fact that they have a relatively spherical bulge at their center made up of superimposed stars. Around this, there is a highly flattened disk made up of spiral arms where young massive stars are generally found. The aspects taken into account for the classification of spiral galaxies is the presence or absence of a bar-shaped feature, how prominent is the bulge, how open or closed are the spiral arms, and the alignment or not of the arms by discrete, resolved objects. There seems to be a correlation between the last three aspects: the arms of galaxies that have large bulges are smooth and tightly wrapped, while the arms of those galaxies whose bulge is small or do not have are patchy and open. Analyzing these characteristics, we came to the classification of Sa, Sb, Sc spirals, with “a” being most tightly

ⁱ<http://stdata.stsci.edu/cgi-bin/dssform>



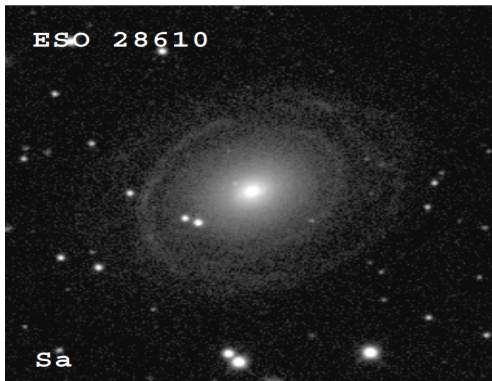
(a) M32 classified as E2 galaxy



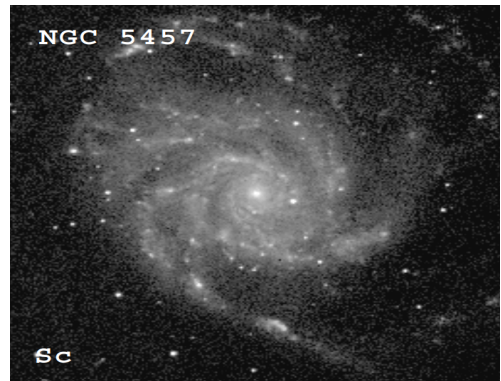
(b) M59 classified as E5 galaxy

Figure 1.3: Examples of elliptical galaxies.

wound². Figure 1.4 shows two examples of spiral galaxies: ESO 28610 classified as Sa galaxy, and NGC 5457 classified as Sc galaxy².



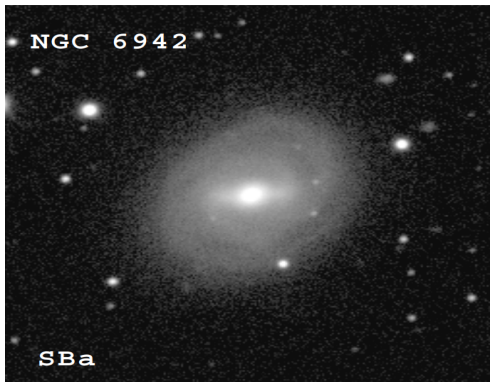
(a) ESO 28610 classified as Sa galaxy



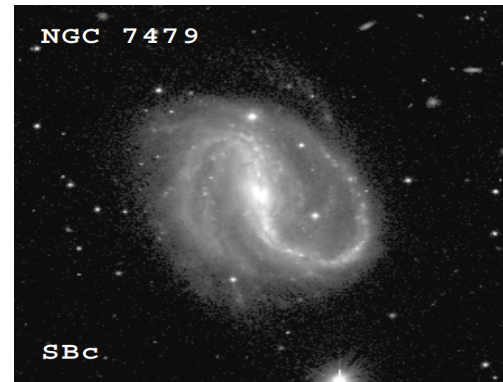
(b) NGC 5457 classified as Sc galaxy

Figure 1.4: Examples of spiral galaxies.

- **Barred Spiral Galaxies (SB):** the main characteristic of this type of galaxy and what sets it apart from normal spirals is that barred spirals have a bright bar of gas at their center. In addition, its spiral arms are broken from the ends of the bar, whereas in normal spirals they are broken from the bulge region. Figure 1.5 shows two examples of barred spiral galaxies: NGC 6942 classified as SBa galaxy, and NGC 7479 classified as SBc galaxy².
- **Irregular Galaxies (I):** as mentioned before, it was initially believed that these types of galaxies did not have a rotational symmetry. However, many are now known to rotate and have bar-shaped structures on their discs.



(a) NGC 6942 classified as SBa galaxy



(b) NGC 7479 classified as SBc galaxy

Figure 1.5: Examples of barred spiral galaxies.

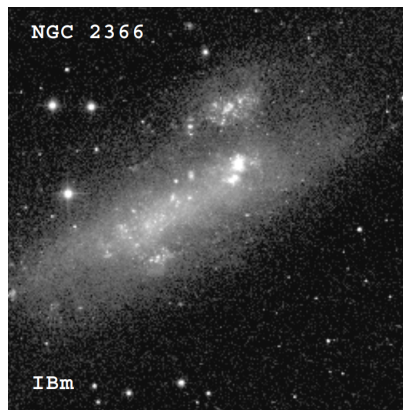


Figure 1.6: Example of irregular galaxy

In addition, its main characteristics is that they do not have a visible nucleus and / or a symmetrical shape. An example of this type of galaxy is NGC 2366 shown in Figure 1.6².

Nearby galaxies and galaxies in the distant universe have a different morphology. Nearby galaxies are those that have a redshift (z) as low as $z = 0.3$ which corresponds to ~ 3.5 Gyr in the past which is barely $\sim 25\%$ of the universe's current age. Galaxies with $z = 0.5$, which corresponds to ~ 5 Gyr in the past, are more chaotic and have less developed spiral arms, and it is rare to find barred spiral galaxies. On the other hand, those galaxies with $z = 1$ are very peculiar, and in the classification system proposed by Edwin Hubble no longer applies⁸. The three galaxies studied in this work are classified as nearby galaxies, that is, they have a very small redshift as can be seen in Table 2.1. For this reason, we are going to focus only on this type of galaxies.

Years after the proposal to classify galaxies according to their morphology, astronomers, specifically Carl Seyfert,

(a) M 74 as example of a face-on spiral galaxy¹¹.(b) NGC 891 as example of an edge-on spiral galaxy¹².

Figure 1.7: Examples of galaxies whose orientation towards the observer varies (face-on and edge-on spiral galaxies).

added another type of classification. In 1943, Carl Seyfert, while conducting a study of galaxies, found that some of the spiral type had a brighter nucleus than normal and their spectrum showed strong emission lines⁹. Seyfert first identified six galaxies with these characteristics and discovered that the main difference between them was their spectrum, more specifically the spectral width of the emission lines. Those galaxies that had wide lines in their spectrum were galaxies whose nucleus could be directly observed (full face-on view, see Figure 1.7a) and were classified as Seyfert 1 AGN. Whereas galaxies that had thin lines on their spectrum were galaxies whose view of the nucleus was hampered (edge-on view, see Figure 1.7b) and were classified as Seyfert 2 AGN¹⁰.

After the study carried out by Seyfert in 1943, it was not clear what the reason was or what caused the nucleus of the studied objects to have these very peculiar spectra. However, in the 1950s, with the advances in radio astronomy, a new universe of energy phenomena was revealed, and with this, the study of Active Galactic Nucleus (AGN) became more important among astronomical observers and theorists¹³. The term AGN refers to the fact that at the nuclei of galaxies there is a peculiar energy phenomenon that cannot be attributed to the existence of stars. The explanation, which until today is accepted, about the emission source of an AGN is the presence of a supermassive black hole located in the nucleus of a galaxy. For the supermassive black hole to produce this nuclear activity, it must be fed by some mechanism that eliminates the angular momentum of the gas that surrounds it¹⁴.

AGNs are divided into two subclasses: Seyfert galaxies (explained above) and quasars. The main difference between these two subclasses is related to the amount of radiation that is emitted by the nucleus or the central part of the galaxy. For instance, the total energy emitted by the nucleus of a typical Seyfert galaxy is similar to the energy emitted by all the stars that make up this galaxy (i.e., $\sim 10^{11}L_{\odot}$). However, the brightness of the nuclei of a typical quasar is greater by a factor of 100 or more compared to the brightness of the stars that compose it¹⁵.

1.2 Star formation, nuclear activity, and molecular gas

Knowing how stars form has been one of the most studied problems in contemporary astrophysics. This is because the formation of stars will determine the structure and evolution of galaxies. Furthermore, most of the chemical elements, even those that make up the world around us, are formed in the stars. On the other hand, the formation and early evolution of planetary systems are extremely linked to the star formation process.

In 1974, Kahn¹⁶ said that star formation can be divided into two parts: low and high mass star formation. The formation time of low-mass stars is less compared to the Kelvin-Helmholz time ($t_{KH} = Gm_*^2/RL$), while the time for high-mass stars is greater than t_{KH} . However, this statement is not fully valid because a high enough accretion rate can cause any protostar to be classified as “low mass”. For this reason, a more appropriate distinction to divide these two types of star is a mass of $8M_{\odot}$. The luminosity source of the stars will depend on the mass of the initial protostar. For instance, the luminosity of stars with masses significantly less than $8M_{\odot}$ is to be dominated by accretion, and the cores from which they are to be formed have masses of the order of the thermal Jeans mass. Likewise, the luminosity of protostars having a mass greater than $8M_{\odot}$ will be dominated by nuclear burning as long as the accretion rate is low. If the accretion rate is very high, its formation will be from molecular cores whose mass is greater than the thermal Jeans mass¹⁷.

The evolution in the Hertzsprung-Russell diagram of low-mass stars is extensive. They start at the “birthline” where they stop accreting and start heading towards the main sequence. The following briefly describes how these types of stars form.

1.2.1 Definition of star formation

In 1987, Shu et al.³ developed a theory about the star formation process which is accepted to this day. They defined four stages of star formation which are represented in Figure 1.8. In the first stage slowly rotating nuclei of molecular clouds are formed due to the loss of turbulent and magnetic support through ambipolar diffusion. In the second stage, the cloud core becomes gravitationally unstable and begins to collapse dynamically from “inside-out”, thus forming a central protostar and a disk enveloped by a cloud of gas and dust. All this gas and dust will help increase the mass of the protostar nucleus. However, the fall of this incoming material is preferably on the disk instead of the core itself due to centrifugal forces and gravitational attraction. Some of the material that is accreted in the disk escapes from the nucleus of the protostar in a direction perpendicular to the disk. In this way, a bipolar flow is created that represents the third stage of formation. In the fourth stage, the fall of the material (gas and dust) ends and a newly formed star with a circumstellar disk is obtained (this disk is known as accretion disk). Finally, a fifth stage can be added where due to the accumulation and elimination of the circumstellar disk planets or stars smaller than the main one are formed³.

1.2.2 Molecular clouds and their connection with star formation

The high density of a region in the Interstellar Medium (IM) makes possible the formation of molecules since this environment is suitable for collisions between atoms to happen more frequently. However, due to the presence of

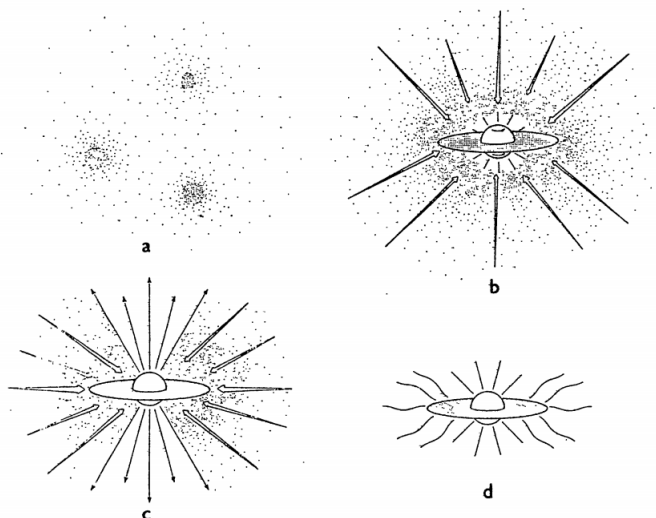


Figure 1.8: Stages of the star formation proposed by Shu et al.³ a) Formation of slowly rotating nuclei from molecular clouds. b) Formation of a central protostar and a disk due to gravitational instability. c) Creation of a bipolar flow due to the accretion of the material. d) End of material fall creating a new star with a circumstellar disk.

UV photons in this medium, the molecules that form by collision between two atoms can be easily dissociated. Interstellar dust serves as protection to prevent this dissociation as it effectively absorbs UV radiation. The main components of this interstellar dust are molecules of carbon (C), silicon (Si), H, O, Mg, Fe, among other elements in the form of ices, silicates, graphites, metals, and other organic compounds¹⁸.

Molecular clouds are the coldest and densest regions of the IM and have two main factors or characteristics for the production and preservation of molecules. These factors are the presence of dust grains and high density. It is important to study the molecular clouds of a galaxy since it is in these regions that the star formation process takes place. In this way, it is possible to know what the initial conditions were so that, through a process of gravitational collapse, new stars can form⁵.

Molecular clouds are characterized by being very inhomogeneous objects since their size can vary from 10 pcⁱⁱ to 100 pc, and their mass can be between $10^2 M_{\odot}$ and $10^7 M_{\odot}$. The main component of a molecular cloud ($\sim 99\%$) is a neutral heterogeneous gas whose density (n) is from 10^2 to 10^6 particles per cubic centimeter. In addition, its kinetic temperature (T_K) ranges from 10 to 100 K. Approximately, 75% of the gas mass is made up of molecular hydrogen (H_2), and approximately the remaining 25% is atomic helium (He). However, there are atomic and molecular species in minimal proportions in which hydrogen is combined with minor elements of the IM such as oxygen, carbon, nitrogen, sulfur, silicon, among others. On the other hand, the remaining 1% of the mass of the molecular cloud is made up of a set of solid grains whose diameter is between a few tenths of a micron and some angstroms, this is known as interstellar dust¹⁹.

ⁱⁱThe parsec (pc) is an astronomical unit of length which is equal to 3.26 light years

1.2.3 Local Thermodynamic Equilibrium

When talking about thermodynamic equilibrium it means that there is a balance between radiation and matter that is located within an ideal cavity and that is used to define the theoretical properties of a black body²⁰. One of the parameters that is used to study the physical properties of stellar objects is temperature. Different types of temperature measurements can be performed depending on the physical processes involved, which are described below²¹:

- **Effective Temperature:** obtained from the Stefan-Boltzmann law described by equation 1.1, where L is the luminosity, R is the radius of a spherical star, σ is the Stefan-Boltzmann constant which has a value of $\sigma = 5.670400 \times 10^{-8} \text{ Wm}^{-2}\text{K}^{-4}$, and T_e is the effective temperature.

$$L = 4\pi R^2 \sigma T_e^4 \quad (1.1)$$

- **Excitation Temperature:** defined by the Boltzmann equation 1.2, which describes the ratio of the number of atoms N_b in a state of energy E_b to the number of atoms N_a in a state of energy E_a in different states of excitation, T is the common temperature of the two systems, the term $e^{-E_i/kT}$ is known as the Boltzmann factor, and g_i is the number of states with energy E_i (degenerate states).

$$\frac{N_b}{N_a} = \frac{g_b e^{-E_b/kT}}{g_a e^{-E_a/kT}} = \frac{g_b}{g_a} e^{-(E_b-E_a)/kT} \quad (1.2)$$

- **Ionization Temperature:** defined by the Saha equation (1.3) which describes the ratio of the number of atoms in stage $(i + 1)$ to the number of atoms in stage i .

$$\frac{N_{i+1}}{N_i} = \frac{2Z_{i+1}}{n_e Z_i} \left(\frac{2\pi m_e kT}{h^2} \right)^{3/2} e^{\chi_i/kT} \quad (1.3)$$

- **Kinetic Temperature:** contained in the Maxwell-Boltzmann distribution (1.4) which describes the number of gas particles per unit volume having speeds between v and $v + dv$.

$$n_v dv = n \left(\frac{m}{2\pi kT} \right)^{3/2} e^{-mv^2/2kT} 4\pi v^2 dv \quad (1.4)$$

- **Color Temperature:** obtained by fitting the shape of a star's continuous spectrum to the Planck function (1.5).

$$B_\lambda(T) = \frac{hc^2/\lambda^5}{e^{hc/\lambda kT} - 1} \quad (1.5)$$

Although all the temperatures mentioned above are defined in different ways, they all have the same value if the simple case of a gas confined within an "ideal box" is studied. In this "ideal box", the confined gas particles and blackbody radiation will come into equilibrium which means that there is no net flow of energy through the box or between the matter and the radiation occurs. This condition is known as thermodynamic equilibrium. However, a star is not in a perfect thermodynamic equilibrium since its temperature varies depending on the location. The photons

and gas particles that are in a certain position in the star had to come from another region with either hotter or colder temperatures, which means that the “ideal box” no longer exists. However, this ideal case in which you have a single temperature can still be applied if the distances traveled by the particles and the photons between collisions (mean free paths) are small compared to the distance over which the temperature changes significantly. If that condition is met, it can be said that we are in Local Thermodynamic Equilibrium (LTE). In this case, the local environment does not allow photons and particles to escape, effectively delimiting them in a limited volume (an approximated “box”) whose temperature is almost constant²¹.

1.2.4 Molecular emission

The densities of the IM are extremely low compared to the terrestrial densities. For this reason, in the IM there are no chemical reactions involving three or more gas particles simultaneously. In addition, the temperature of the molecular clouds is so low that endothermic reactions (those that require energy input to perform) are generally irrelevant. In this way, the fundamental mechanism for the formation of molecules in the IM are ion-molecule reactions. In this type of reactions one of the involved particles is charged (ions). Ions can exist in molecular clouds because cosmic rays penetrate the cloud.

To date, a hundred molecular species have been identified in the interstellar and circumstellar medium, which are listed in Table 1.1. These species range from simple diatomic molecules like carbon monosulfide (CS) to molecules that have fifteen atoms like $HC_{13}N$. Most of these molecules have a linear structure. However, a few molecules have a cyclic structure and are indicated in square brackets in Table 1.1.

1.2.5 Dense gas tracer molecules

Despite the fact that molecular hydrogen (H_2) is the most abundant compound in the molecular medium, it is not a good molecular cloud tracer since, because it is made up of two identical atoms, its radiative transitions are very slow and can hardly be detected. Carbon monoxide (CO) is the second most abundant compound in IM and, due to its molecular structure, the transition between its two lowest rotational levels can be observed, line $J = 1-0$ (115 GHz), as long as the density of the gas is several hundred particles per cubic centimeter. This last condition is fulfilled in practically all molecular clouds. For this reason, $CO(1 - 0)$ is an excellence tracer of the molecular medium. Furthermore, this molecule faithfully traces the entire molecular mass regardless of the conditions in which the cloud is. However, the molecule by itself does not contribute relevant information about the physical conditions of the molecular medium¹⁹. For this reason, it is necessary to resort to the study of other molecular species that provide this type of information, which will be detailed below:

- The most frequently observed dense gas tracer molecular species is HCO^+ whose simplest transitions $J = 1-0$ (89 GHz) is only detectable when the gas density is $\gtrsim 10^4 \text{cm}^{-3}$. From now on, each time this last characteristic is fulfilled, it will be considered as dense gas¹⁹. HCO^+ forms in dense molecular clouds mainly through the reaction $H_3^+ + CO \rightarrow HCO^+ + H_2$ ²². In regions where shocks are generated, the abundance of this molecule may increase due, for example, to the presence of flows from Young Stellar Objects (YSO)

Hydrogen Molecules							
H_2	H_2D^+						
Carbon Molecules							
C_2	CH^+	C_3	C_4	C_5	CH	C_2H	C_3H
C_4H	C_5H	C_6H	CH_3C_2H	CH_3C_4H	CH_4	C_2H_2	
C_2H_4	$[C_3H_2]$	$[C_3H]$	H_2C_3	H_2C_4			
Oxygen Molecules							
CO	CO^+	CCO	C_3O	C_5O	OH	H_2O	H_3O^+
HCO	HCO^+	HOC^+	$HOCO^+$	H_2CO	CH_3CHO	CH_3OH	CH_3CO
CH_3HCHO	$(CH_3)_2CO$	CH_3OCH_3	$HCOOCH_3$	CH_3CH_2OH	HC_2CHO	$HCOOH$	C_2H_2O
Nitrogen Molecules							
CN	C_3N	HC_3NH^+	$HCCN$	$HCCNC$	$HNCCC$	HCN	HC_3N
HC_5N	HC_7N	HC_9N	$HC_{11}N$	$HC_{13}N$	HNC	NH	NH_3
N_2H^+	CH_3CN	CH_3NC	$HCNH^+$	NH_2CN	CH_2CN	CH_2NH	CH_3NH_2
CH_3CH_2CN	CH_2CHCN	CH_3C_3N	CH_3C_5N	NO	HNO	$HNCO$	$HOCN$
NH_2CHO							
Sulfur, Silicon or Phosphorus Molecules							
SO	SO_2	NS	H_2S	OCS	HCS^+	CS	C_2S
C_3S	SO^+	H_2CS	$HNCS$	CH_3SH	PN	CP	CP
SiC							
SiO	$[SiC_2]$	SiS	SiN	SiH_4	$HSiCC$	SiC_4	
“Metallic” Molecules							
HCl	$NaCl$	KCl	$AlCl$	AlF	$NaCN$	$MgNC$	

Table 1.1: List of detected molecules in the interstellar and circumstellar medium so far. The molecules in square brackets have a cyclic structure, and the others have a linear one⁵.

immersed in dense gas²³. The HCO^+ molecule can also be formed from the H_2O molecule following the reaction $C^+ + H_2O \rightarrow HCO^+ + H^{24}$. On the other hand, its destruction is mainly caused by recombination with electrons, $HCO^+ + e^- \rightarrow CO + H$.

- **HNC** molecule abundance is known to be low in high temperature regions but abundant in dark (dense) molecular clouds²⁵. Besides, the influence of UV radiation can be one of the causes of a bright *HNC* emission in PDRs and / or X-rays in XDRs areas whose densities are $n \gtrsim 10^4 \text{cm}^{-3}$, and have a column density of $N_H > 3 * 10^{21} \text{cm}^{-2}$ ²⁶. The metastable geometric isomer of this molecule is **HNC**, which also happens to be a dense gas tracer in molecular clouds, and is especially prevalent in cold gas. The **HNC / HCN** ratio has been predicted to be ~ 0.9 ²³.
- **HNCO** and **CH₃OH** molecules are typical species that are related to shocks regions. The *CH₃OH* molecule can also be detected in hot cores, making it a good dense gas tracer²⁷. On the other hand, Rodriguez- Fernández et al 2010²⁸ demonstrated that the abundances of *HNCO* measured in galactic nuclei can be produced by shocks, and proposed that the gaseous phase of *HNCO* can be produced by two mechanics:
 1. Grain mantle erosion by the shock waves.
 2. Neutral-neutral reactions in gas phase involving *CN* and *O₂*.
- It is presumed that water and methanol molecules are abundant in the shock regions of the molecular cloud. For this reason, the H_3O^+ and $CH_3OH_2^+$ ions are expected to be formed rapidly, and these in turn will produce N_2H^+ and HCO^+ . However, because electron abundance can increase in the shock zone due to partial ionization of the medium, it is highly likely that these ions are rapidly destroyed by dissociative recombination²⁷.

1.3 Problem Statement

The study of the molecular medium is essential to understand the process of star formation in galaxies. Molecular gas is the fuel of the star formation, therefore multi molecular line observations and their analysis are crucial for understanding the physical and chemical conditions of galaxies, which provide key information about how star formations is triggered.

However, the molecular gas properties are also affected by the nuclear activity. Some studies in local galaxies suggest that the molecular gas properties in galaxies (abundances, densities, gas temperature, etc.) could be different between Starbursts (SB) and AGN dominated objects. The presence of a nuclear SB or an AGN could create quite different chemical and physical conditions for the molecular gas in galaxies. The analysis of the molecular lines would help to discriminate

1.4 General and Specific Objectives

1.4.1 General Objective

The purpose of this work is to analyze the molecular gas in three local galaxies with different kind of nuclear activity, with the aim of understand better the AGN-SB connection. The three galaxies were observed with the wide-band (30 GHz) facility RSR at the “Gran Telescopio Milimetrico Alfonso Serrano” (GTM, Sierra Negra, Mexico) in the spectral window of 3 mm. Besides, they show a rich molecular spectra, which will allow a deep analysis of the dense molecular medium for these galaxies.

1.4.2 Specific Objectives

- Identify the molecular species of the spectra of each galaxy.
- Estimate the columnar densities of the identified molecular species.
- Compare the columnar densities between the galaxies in my sample to identify which molecules are characteristic of one or another nuclear activity.

The structure of this work is as follows: in Chapter 1, a brief introduction to fundamental topics and concepts for the development of the thesis is shown. Some of the topics addressed in this chapter are star formation, nuclear activity, molecular clouds, and molecular species tracers of dense gas. This last topic is the most important since it will give information about the physical processes that are occurring in each of the galaxies studied in this work. In Chapter 2, the methodology used to achieve the proposed objectives is described. The general information and characteristics of each of the galaxies, information about the telescope with which the observations were made, and the process of data reduction are shown. Chapter 3, shows the results obtained from the analysis of the spectral lines of the molecular clouds of the three galaxies, together with their respective discussion. In addition, the spectrum of each galaxy is shown with their respective identified molecular species and their column densities. In Chapter 4, the analysis, comparison, and discussion of the results obtained in Chapter 3 are carried out. Finally, in Chapter 5 the conclusions of the thesis and its future work are shown.

Chapter 2

Methodology

2.1 The sample of the galaxies

On this work, we selected a sample of three galaxies to study their dense molecular gas properties which share similar characteristics. For instance, the three galaxies are spirals and face-on galaxies. They are in the local universe, this mean that their redshift (z) is less than 0.05, and their distance (D) is less than 200 Mpc²⁹. Due to they are nearby galaxies, we can assume that we are seeing only the central part of the galaxy, that is, its nucleus. Another advantage of having nearby galaxies is that the observation will be better since the telescope will capture more number of photons and the spectrum will be more intense. In the same way, when we study galaxies that have the same or very similar redshift we make sure that we are seeing the same region in all galaxies. In the same way, when we study galaxies that have the same or very similar redshift we make sure that we are seeing the same region in all galaxies. This allows that when making the comparison between galaxies this is making between similar things and objects. Moreover, the galaxies have the same rms and infrared luminosity. However, there is a characteristic that makes them different, which is their nuclear activity which makes them suitable for the purpose of the development of this work. For this reason, when the study about nuclear activity is carried out, we will be certain that no other characteristic will influence. In our sample we include two AGNs as are NGC 4414 and NGC 4826, and a Starbursts galaxy as NGC 2903. You can see the main characteristics of these three galaxies in Table 2.1.

2.1.1 NGC 4826

NGC 4826 (M64) is a nearby galaxy classified as a Seyfert by their nuclear activity, or as a SABA³⁰ galaxy by their morphology. This galaxy is alternately referred to as the “Evil Eye”, “Black Eye”, or “Sleeping Beauty” because near its bulb on the northeast side there is a prominent dust lane³¹. Dense gas tracers of this source (HCN (1-0) and HCO^+ (1-0)) were reported by Krips et al.(2008)³², as well as their respective ratios. HCO^+/HCN 1-0 line ratio is 0.59 ± 0.04 . Also, Casoli Gerin(1993)³³ reported the ^{13}CO line at $J = 1-0$.

Table 2.1: Galaxies Properties.

		NGC4826	NGC2903	NGC4414
		M64		
Right Ascension	(J2000)	$12^h56^m43.696^m$	$09^h32^m10.111^s$	$12^h26^m27.089^s$
Declination	(J2000)	$+21^\circ40'57.57''$	$+21^\circ30'02.99''$	$+31^\circ13'24.76''$
Object Type		(R)SA(rs)ab	SAB(rs)bc	SA(rs)c
Distance	(Mpc)	4.7 ^a	9.3 ^c	18 ± 3.0
Redshift (z)		0.00136	0.00183	0.00239
Star Formation Rate	($M_\odot yr^{-1}$)	0.2	2.9 ^d	3.45 ± 1.58
Inclination Angle	(Degrees)	60	67.1 ^c	55 ^b

Most of the information in this table was collected from: Hubble Space Telescope, SIMBAD astronomical database, and NASA / IPAC Extragalactic Database (NED), except for those listed bellow.

^a Jacobs et al. (2009)³⁷.

^b Vallejo et al. (2002)³⁸.

^c Makarov et al. (2014)³⁹.

^d Heesen et al. (2014)⁴⁰.

2.1.2 NGC 2903

NGC 2903 is a nearby spiral galaxy classified as SAB(rs)bc. Topal (2018)³⁴ states that this galaxy is a good candidate to better understand the differences in the star formation processes, and the effects that this has on the ISM in the starburst galaxies. Besides, he reported the integrated intensities of ^{13}CO (1-0) and HCN (1-0) lines which is 1.99 ± 0.45 and 3.21 ± 0.65 (K km/s) respectively, the total molecular gas mass in the unit of solar mass is $M_{H_2} = (3.80 \pm 0.12) * (10^7 M_\odot)$, and the beam-averaged H_2 column density is $N(H_2) = (5.26 \pm 0.46) * (10^{21} cm^{-2})$. In the same way, Vila-Vilaro et al.(2015)³⁵ also reported the integrated intensities of ^{13}CO (1-0) with a value of 2.01 ± 0.11 (K km/s).

2.1.3 NGC 4414

NGC 4414 is a unbarred SA(rs)c late-type galaxy which shows patchy spiral arms and star formation³⁶. This galaxy is an excellent candidate for dynamical measurements due to its undisturbed dynamical features. Performing a literature search within NASA's Astrophysics Data System (ADS), no evidence has been found that this galaxy has been observed within the 3 mm band in a frequency range $\sim [73 - 111]$ GHz. For this reason, there are no measurements and line detections of this galaxy.



Figure 2.1: General map of Mexico showing the site of the Large Millimeter Telescope (LMT) which is located near the city of Puebla.

2.2 Description of the telescope (LTM) ⁱ

The observations presented in this work were carried out with the Large Millimeter Telescope (LMT) Alfonso Serrano or “Gran Telescopio Milimétrico Alfonso Serrano”. It is the world’s largest single-dish steerable millimetre-wavelength telescope, and works developing astronomical observations in the wavelength range from 0.85 to 4 mm. It is situated on the summit of Volcán Sierra Negra at an altitude of 4600 meters (Fig. 2.1). This project was born with the collaboration of the University of Massachusetts Amherst (UMass Amherst) in the United States and the Instituto Nacional de Astrofísica, Óptica y Electrónica (INAOE) in Mexico.

The LMT study objective ranges from physical processes that lead to the formation and evolution of planetary systems to the study of stars and galaxies with different types of nuclear activity. In order to study all these objects, radio telescopes must not only collect information in large areas on the earth’s surface, but they must also be equipped with extremely sensitive electronic devices. It is impossible to buy all these equipment, receivers and spectrometers with such specifications. For this reason, it is necessary that they be personally developed and constructed by the institutes involved in the project. In addition to sensitive equipment, the accuracy of the primary mirror (the plate) of the 50 m LMT must be invariant under distorting effects due to gravity and thermal gradients. The precision must be more than 1 second of arc, and to have a reference and better understand this term it is as if we wanted to hit a dime at a distance of 2 km. It should be noted that no other telescope can aim with such precision.

ⁱThe information in this section was obtained from⁴¹.

2.2.1 Antenna

The LMT began operating with a surface of 32 m. However, from 2018 it operates with an active primary surface of 50 m in diameter, which makes it operate with excellent efficiency at wavelengths as short as 0.8 mm. The main specifications about the 50 m LMT are indicated in the Table 2.2, and in Figure 2.2 you can find a Schematic diagram of the LMT.

Table 2.2: Main specifications of the LMT.

Property	Specification
Effective Surface Accuracy	75 μm rms
Pointing Accuracy	1.0 arcsec
Aperture Efficiency (3.0 mm)	0.65
Aperture Efficiency (1.2 mm)	0.40
Sensitivity (3.0 mm)	2.2Jy/K
Sensitivity (1.2 mm)	3.5 Jy/K
FWHM beam size (3.0 mm)	15 arcsec
FWHM beam size (1.2 mm)	6 arcsec

One of the challenges of building a single dish antenna is achieving great precision on its surface. Comparing the precision of other telescopes with the LMT the improvement is evident due to the implementation of 180 moving surface segments. A very rigid reaction structure is supporting each of the segments and by means of an spatial frame it is attached to a posterior structure of the reflector. Each spatial frame can be adjusted to the posterior structure by means of four actuators that help correct possible deformations that can be generated by gravity and/or thermal gradients. All relevant parts of the structure have temperature sensors that are connected to the control system. Simulations performed show that the LMT in the presence of winds up to 10 m / s should be able to maintain surface precision.

2.2.2 Instrumentation

The LMT works in two different ways: spectroscopy and continuous. On the one hand, spectroscopy analyzes the detected radiation to measure the intensity of the signal as a function of frequency or wavelength. On the other hand, in continuous systems the total amount of received energy is measured within a wide frequency range. Due to the LMT collection area is approximately 2000m², and it has an excellent surface precision, the sensitivity of the telescope greatly exceeds the existing telescopes that also work in mm wavelengths. Furthermore, this sensitivity is improved in continuous observations due to the ability of the single dish to use very wide bandwidth incoherent detectors (bolometers). For these reasons, the LMT is a very valuable complement worldwide for mm wave facilities.

In order to keep the LMT in the forefront in future years, a joint work between UMas Amherst and INAOE must be implemented to continue developing new instruments.

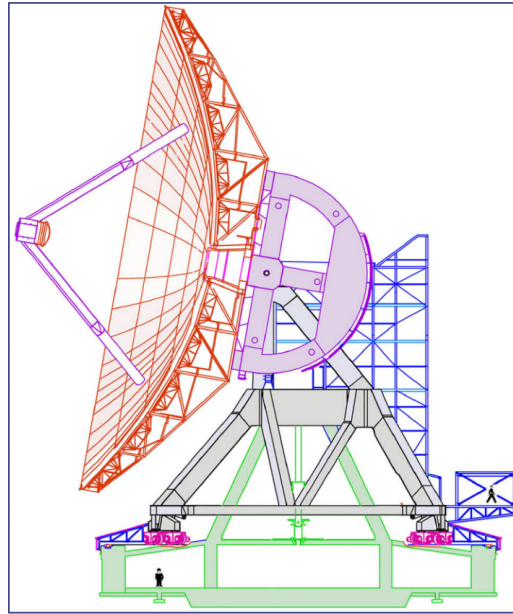


Figure 2.2: General scheme of the Large Millimeter Telescope (LMT).

When the LMT operated with 32m, it consisted of two instruments: Redshift Search Receiver (RSR) and Astronomical Thermal Emission Camera (AzTEC). The RSR is a broadband spectrograph whose specifications will be detailed later since it is the instrument with which the observations for this work were made. On the other hand, as mentioned before, the sensitivity of the telescope can be improved by continuous observation using incoherent wide band detectors. These detectors are known as bolometers and are the most optimal method for observing the continuous emission of dust particles or charged particles of high energy. The LMT will have a sensitive bolometer called AzTEC. This can operate in 2.1 and 1.1 mm bands and provides 144 pixels. In addition, its use is mainly aimed at searching for newly formed galaxies in the young universe, identifying protostellar nuclei in molecular clouds, studying dust in galaxies using astrochemistry, and studying comets and asteroids in the solar system.

As of 2018, with the LMT with 50m, other instruments such as SEcond QUabbin Optical Imaging Array (SEQUOIA) and TolTEC began to work.

SEQUOIA is a 32-pixel, dual polarization heterodyne focal plane array which is already completed and operating in the Five College Radio Astronomy Observatory (FCRAO) 14 m telescope for spectroscopy in the 85-115 GHz frequency band. UMass Amherst has also developed the second receiver system for use in the 3 mm band. The main feature of this ultra-wideband receiver/spectrometer is that it covers the range from 75-111 GHz with a 30 MHz spectral resolution. Besides, it can switch rapidly between two positions in the sky with dual polarization feeds. On the other hand, TolTEC is a new millimeter-wavelength camera which has 6300 detectors spread across three different bands (2.0 mm, 1.4 mm, and 1.1 mm). The system that will be produced by the combination of TolTEC with the LMT will be capable of mapping the sky with a resolution of up to 5 arcseconds and its mapping speed will

be up to 10 square degrees/square mJy/hr. These characteristics make this new instrumentation more than 100 times faster than the AzTEC camera which is currently mapping the sky in the LMT⁴².

Nowadays, the instruments with which the LMT operates have been successfully tested and used in other (sub) millimeter (14 m FCRAO, 15 m James Clerk Maxwell Telescope (JCMT), and 10 m) telescopes before coupling to the LMT⁴³. For the development of this work, observations made with the RSR were used, whose characteristics and general information are described below.

Redshift Search Receiver (RSR)

The RSR is an instrument that was designed to maximize the receiver’s instantaneous bandwidth and cover the 90 GHz (73 - 111 GHz) atmospheric window in a single tune. The RSR typically achieves noise temperatures 38 K between 73 and 111 GHz. The RSR provides exceptional baseline stability which allows adequate detection of CO transition lines from galaxies at cosmological distances and with high rates of star formation. The RSR was tested on the 14 m FCRAO in 2006, and in June 2011 the first light demonstration observations at the GTM was performed⁴³. This instrument has four pixels arranged in a dual beam, dual polarization configuration. The frequency range 73 - 111 GHz is covered instantaneously by the four broad-band receivers with a spectral resolution of 31 MHz ($\sim 100\text{km s}^{-1}$ at 93 GHz). The 32-m telescope have an effective beam size of 28 arcsec at 75 GHz and 20 arcsec at 110 GHz⁴⁴.

2.3 Observations and data reduction

2.3.1 Observations

The observations toward three local galaxies were made with the RSR on the 32 meters LMT telescope located on Sierra Negra Volcano in Mexico. The observing run was carried out on different dates for each galaxy as part of a larger project entitled “Analyzing extreme extragalactic objects with GTC, GTM and HAWC”. NGC 2903 was observed on February 1, 9 and 11, 2015 with a total of 2 hours of observation. NGC 4414 was observed on February 23, 2017 for 1 hour. NGC 4826 was observed on February 26 and 27, 2016 for 1 hour and 45 minutes. At that time, the inner 32 m diameter of the surface telescope was working whose effective beam size was 20 arcsec at 110 GHz⁴⁵. The setup of the observations are shown in Table 2.3.

Source	Band Range (GHz)	T_{sys} (K)	Time (min)	Weather conditions	Opacity at 223 GHz
NGC 4826	73 - 111	96-107	1hr 45min	Average	0.16
NGC 2903	73 - 111	96-107	2hr	Good	0.08-0.12
NGC 4414	73 - 111	96-107	1hr	Good Enough	0.06

Table 2.3: Observational Parameters.

2.3.2 Data reduction

Once the observation data has been obtained, the data reduction process and calibration was developed. For doing this, a code written in Python were used which employs the last verions of Data REduction and Analysis Methods in PYthon (DREAMPY). It is a package software written by G. Narayanan with the purposes of calibrating and reducing the LMT-RSR observations. Each spectrum was analyzed separately, and after eliminating bad channels or noise that the spectra may have, the linear baseline of each spectrum was removed.

The reduced spectra of each galaxy were obtained in units of Antenna Temperature scale (T_A^*), which have been corrected for atmospheric losses, scattering, and rear spillover. Figures 2.3a, 2.3b and 2.3c show the resulting spectrum for NGC 4826, NGC 2903, and NGC 4414 respectively.

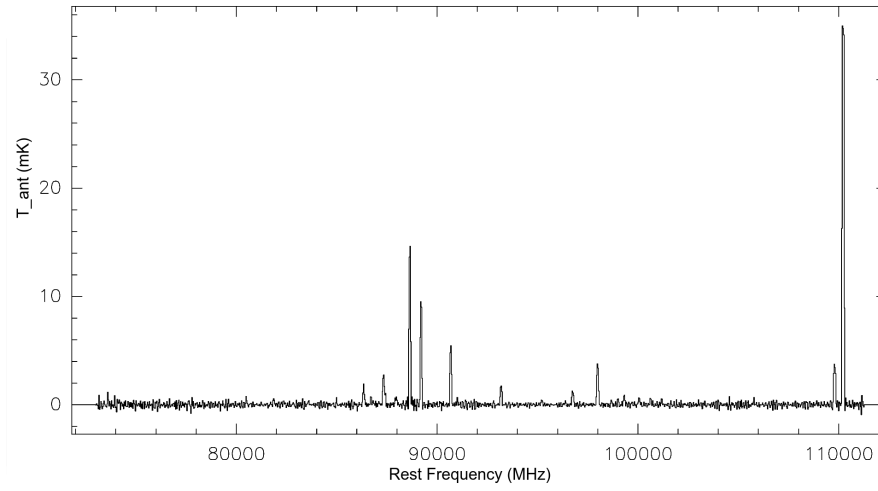
The final spectrum was converted into main beam temperatures (T_{mb}) using the relationship described in equation 2.1, where μ_{mb} is the main-beam efficiency of the telescope. Since the molecular source sizes of the galaxies are not known, the correction of the data was not made according to these parameters.

$$T_{mb} = \frac{T_A^*}{\mu_{mb}} \quad (2.1)$$

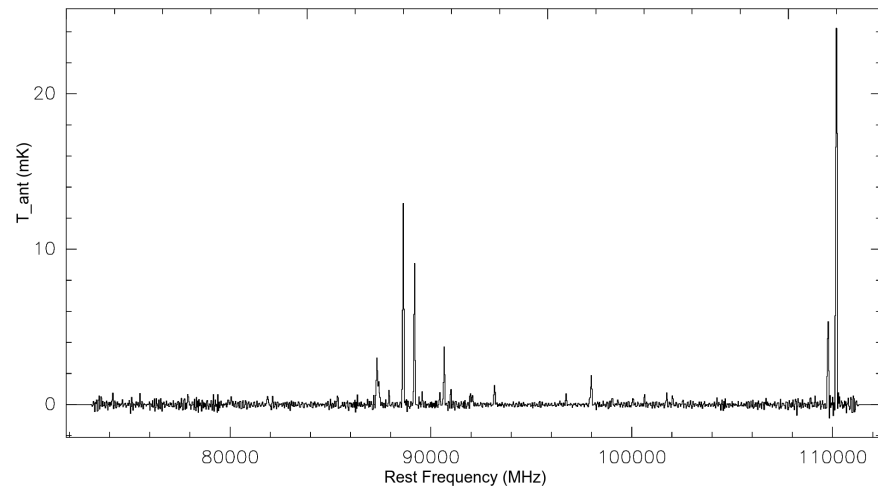
The efficiencies of the main beam (μ_{mb}) will vary according to the observations and the frequency at which it is working. Table 2.4 shows the efficiencies used in this work for each galaxy with its respective frequency range.

	88GHz Region	95GHz Region	100GHz Region
NGC 4826	0.72	0.60	0.70
NGC 2903	0.61	0.50	0.60
NGC 4414	0.72	0.60	0.70

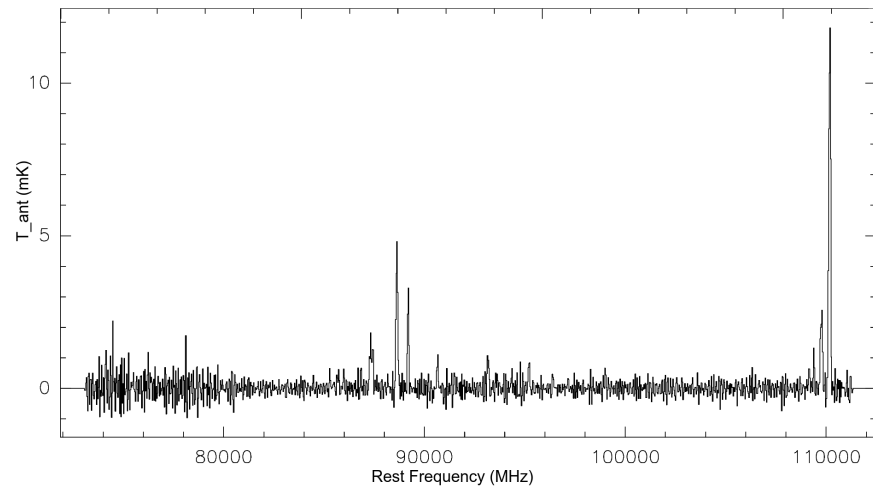
Table 2.4: Main beam efficiencies used in this work.



(a) Reduced spectrum of NGC 4826.



(b) Reduced spectrum of NGC 2903.



(c) Reduced spectrum of NGC 4414.

Figure 2.3: Spectrum of the three galaxies after the reduction process.

Chapter 3

Results

In this chapter, the reduced spectra of each galaxy obtained in the previous chapter will be used to identify the lines and calculate their respective column density. By doing this, I intended to calculate the necessary parameters to characterize the interstellar medium of an AGN and a Starburst-type galaxy.

3.1 Molecular Lines Identification

To identify the molecular lines, I first corrected the observed frequency due to the effect of the redshift of each galaxy (see Table 2.1 to know the redshifts for each galaxy) that is described by equation 3.1:

$$f_{rest} = f_{obs} * (1 + z), \quad (3.1)$$

where f_{rest} is the frequency at rest, f_{obs} is the observed frequency, and z is the redshift.

Then, I plotted these corrected spectra to identify the lines. Each peak in the spectra is known as a *line*. In some cases, these lines are easily identifiable since they are more intense and stand out above the others, such as the line observed at the 110 GHz frequency that corresponds to the ^{13}CO molecule. However, there are faint lines that can be confused with the noise of the observation itself. For these cases, a selection criterion must be applied.

In this work, I consider “detected” lines as those whose peak line value exceeds three times the signal to noise ratio (or rms) of the spectrum. To calculate the rms of each spectrum I used CLASS package of GILDASⁱ. CLASS is a software package whose main objective is the spectroscopy reduction of data obtained apart from observations made with a single-dish telescope. The advantage of this software over others in use is the way in which an observation can be identified. CLASS is very user friendly and uses simple but powerful commands. The rms was calculated for each spectrum, and the procedure was as follows. Once a spectrum was loaded into CLASS, windows should be set in which it was not desired to calculate the rms since within these windows were intense lines that certainly belong to a molecule. In other words, the lines were masked and the adjustment was only made on the continuum.

ⁱ<https://www.iram.fr/IRAMFR/GILDAS/>

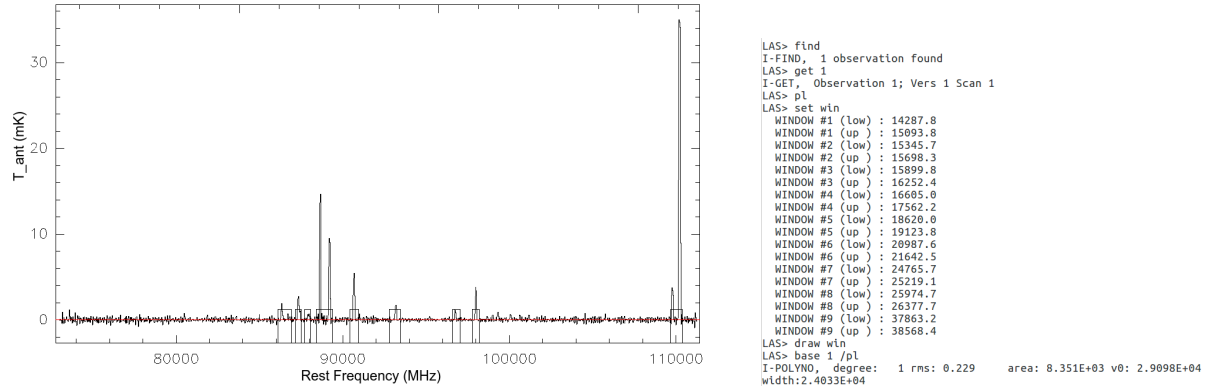


Figure 3.1: calculation of the rms using CLASS.

Source	rms (mK)
NGC 4826	0.22
NGC 2903	0.18
NGC 4414	0.23

Table 3.1: Overall rms of the three galaxies.

Subsequently, the program was instructed to delete a linear baseline of the spectrum, and the value of the rms was dropped. Figure 3.1 shows the procedure to calculate the rms, and table 3.1 shows the overall rms for each galaxy.

Due to the fact that the RSR is composed of six different spectrographs that work in different frequency ranges, each one will generate its own noise, so the rms of each range must be calculated following the aforementioned procedure for the case of the general spectrum. Table 3.2 shows the rms values in intervals corresponding to each galaxy.

After calculating the rms for each galaxy, the lines whose peak intensity value was three times the value of the rms were detected. For the identification of the lines that met this condition, we used the SPLATALOGUE Database for Astronomical Spectroscopyⁱⁱ. It is a very extensive database which contains information of more than 5.8 million of lines. The frequency of each line was searched in this database with an uncertainty of ± 0.3 GHz, and finally the molecules were identified.

Considering these specifications, twenty-three lines of molecular transitions were detected in NGC 4826 belonging to both simple and complex molecules, ^{13}C bearing isotopologues of CO, HCN, HNC, and HCO, the ^{18}O bearing

ⁱⁱ<https://www.cv.nrao.edu/php/splat/advanced.php>

Frequency Range (GHz)	NGC 4826 (mK)	NGC 2903 (mK)	NGC 4414 (mK)
73.063281 - 79.469531	0.255	0.242	0.457
79.363281 - 85.769531	0.192	0.173	0.225
85.630469 - 92.036719	0.247	0.178	0.267
91.959281- 98.365531	0.130	0.103	0.232
98.259281- 104.665531	0.189	0.170	0.221
104.526469- 110.932719	0.232	0.211	0.253

Table 3.2: RMS values in intervals for each galaxy.

isotopologues of CO, the ^{34}S bearing isotopologues of CS. Furthermore, CH_3CN , CH_2CN , $^{13}\text{CH}_3\text{OH}$, H^{13}CN , HN^{13}C , HC_5N , and CH_3OCH_3 were only detected in NGC 4826.

Similarly, twenty-eight molecular transitions were identified in NGC 2903 which makes the galaxy with the largest new species in our sample. The molecules that only were detected in this galaxy were C_4H , CCCN , HC_3N , HNCO , HCCNC , $\text{CH}_3\text{CH}_2\text{CN}$, CH_3OCHO , and AlCl .

In the third galaxy studied, NGC 4414, nine molecular transitions were identified. This is the lower number of identified lines of our sample due to the big noise that its spectrum presents. The only identified molecule different from the other two galaxies is HC_3N (12-11).

Table 3.3 list the detected and non-detected lines of the three galaxies. Moreover, figures 3.2, 3.3, and 3.4 show all the detected lines of NGC 4826, NGC 2903, and NGC 4414 respectively. **It is necessary to mention that it is the first time that most of the molecules detected in this work have been identified in the three galaxies of my sample. For this reason, this is our first important result obtained.**

3.2 Molecular Line Intensities Calculation

Once the lines have been identified, their integrated line intensity was calculated. For this, first, one or more Gaussians were fitted for each line in the spectrum using CLASS. The same program gives the information about the adjusted Gaussian, such as the peak of the curve, their position, and Full width at half maximum (FWHM). In Figure 3.5 an example of how the Gaussian fitting was made and the type of information that CLASS throws is shown.

Now, with the parameters of the Gaussian fitting obtained, I started by calculating the integral of a gaussian (area under the curve) by using the equation 3.2:

$$\int_{-\infty}^{\infty} ae^{-(x-b)^2} dx = ac\sqrt{2\pi}, \quad (3.2)$$

where a is the height of the curve's peak, b is the position of the center of the peak, and c is the standard deviation (σ). For our purpose, the height of the curve's peak is the \mathbf{T}_{mb} peak (calculated in Section 2.3.2), and standard

Molecule	Frequency (GHz)	Transition	NGC 4826	NGC 2903	NGC 4414
CH ₃ CN	73.609227	4 - 3	Yes	-	-
C ₄ H	74.155875		-	Yes	-
CH ₃ OH	75.515475		-	Yes	-
CCCN	79.169895	N=8-7, J=15/2-13/2	-	Yes	-
CH ₂ CN(<i>blend</i>)	80.494678		Yes	-	-
HC ₃ N	81.869064	9-8	-	Yes	-
¹³ CH ₃ OH	84.988973		Yes	-	-
c-C ₃ H ₂	85.351801	2 _{1,2} - 1 _{1,0}	-	Yes	-
H ¹³ CN	86.339372	1-0	Yes	-	-
HCO	86.700076	1 _{0,1} - 0 _{0,0}	Yes	-	-
H ¹³ CO ⁺	86.700076	1-0	Yes	-	-
C ₂ H(<i>blend</i>)	87.338110	1-0	Yes	Yes	Yes
HNCO	87.918158	4 _{0,4} - 3 _{0,3}	-	Yes	-
HNCO + C ₆ H	87.949984		Yes	-	-
HCN	88.632625	1-0	Yes	Yes	Yes
HCO ⁺	89.189937	1-0	Yes	Yes	Yes
HCCNC	89.411150	9-8	-	Yes	-
CH ₃ CH ₂ CN	89.575756	10 _{4,6} - 9 _{4,5}	-	Yes	-
CH ₃ OCHO	90.440818		-	Yes	-
HNC	90.664367	1-0	Yes	Yes	Yes
HC ₃ N	90.992725	10-9	-	Yes	-
CH ₃ ¹³ CN + H	92.012973		-	Yes	-
N ₂ H ⁺	93.168088	1-0	Yes	Yes	Yes
¹³ CH ₃ OH	95.213537	2 _{1,1} - 1 _{1,0}	Yes	-	-
C ³⁴ S	96.418957	2-1	Yes	Yes	-
CH ₃ OH	96.733713	2 _k - 1 _k	Yes	Yes	-
CS	97.983000	2-1	Yes	Yes	-
H	99.033623		-	Yes	Yes
SO	99.315634	3 ₂ - 2 ₁	Yes	-	-
HC ₃ N	100.063197	11-10	Yes	Yes	-
CH ₃ OH	100.633422	13 _{2,11} - 12 _{3,9}	Yes	Yes	-
HC ₅ N	101.189634	38-37	Yes	-	-
CH ₃ OH	101.744215	9 _{-2,8} - 9 _{1,8}	-	Yes	-
AlCl	102.037260	7-6	-	Yes	-
CH ₃ OCH ₃	105.768558	13 _{1,12} - 13 _{0,13}	Yes	-	-
HC ₃ N	109.394234	12-11	-	-	Yes
C ¹⁸ O	109.774078	1-0	Yes	Yes	Yes
¹³ CO	110.191383	1-0	Yes	Yes	Yes

Table 3.3: List of the molecular species identified in the three galaxies. *Yes* and *-* represent the detected and non-detected molecule respectively for each galaxy of my survey.

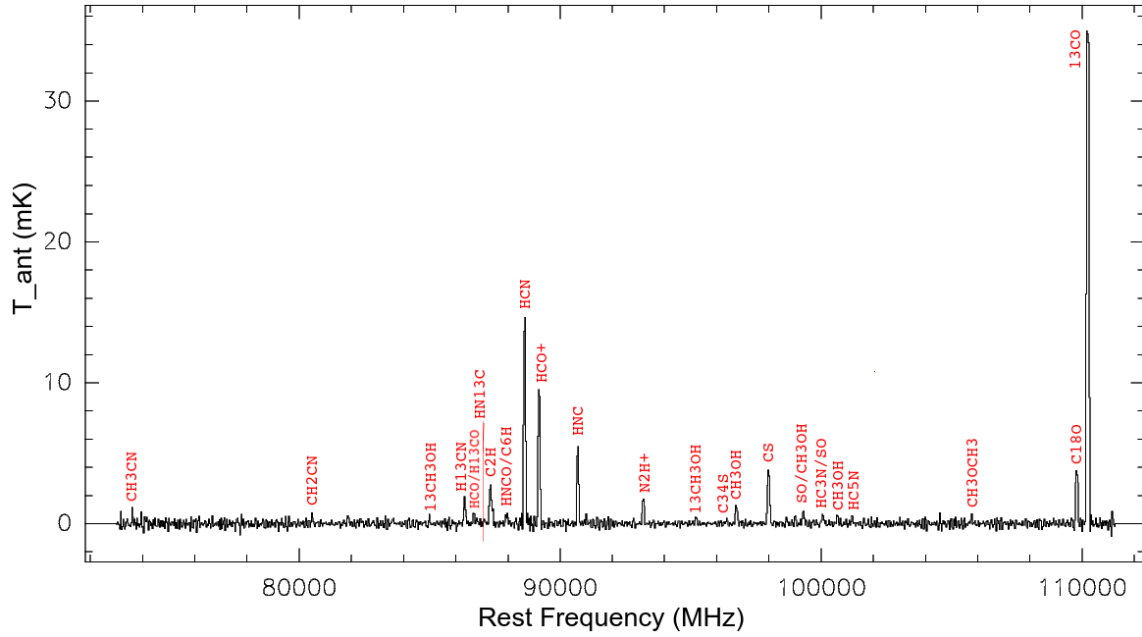


Figure 3.2: NGC 4826 spectrum between 75 and 111 GHz. All the detected species in the galaxy are indicated.

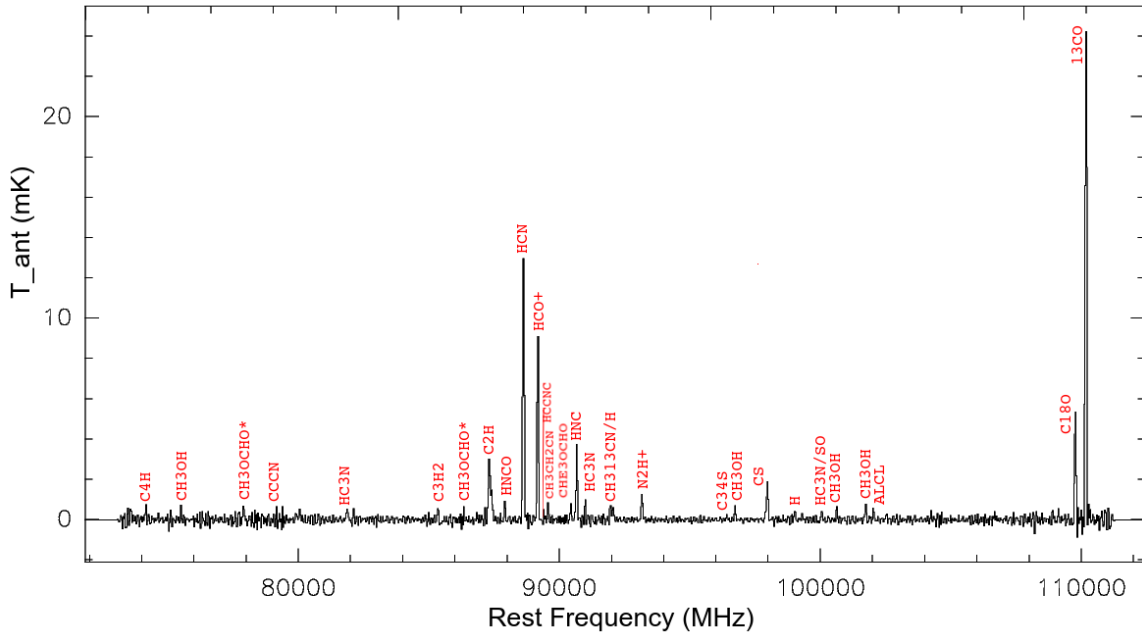


Figure 3.3: NGC 2903 spectrum between 75 and 111 GHz. All the detected species in the galaxy are indicated.

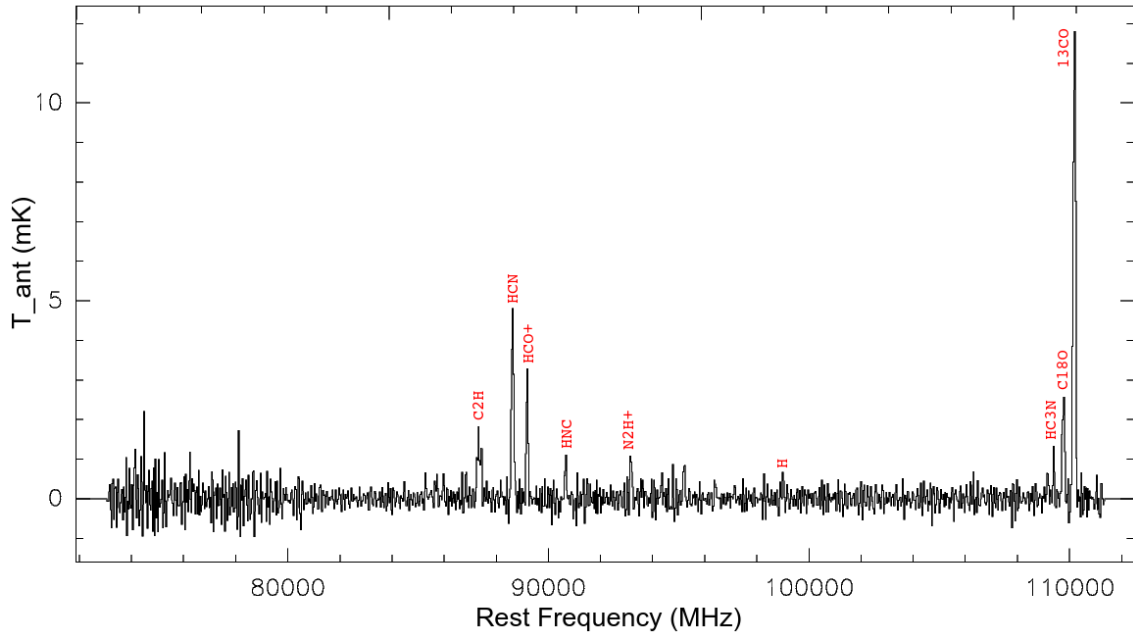
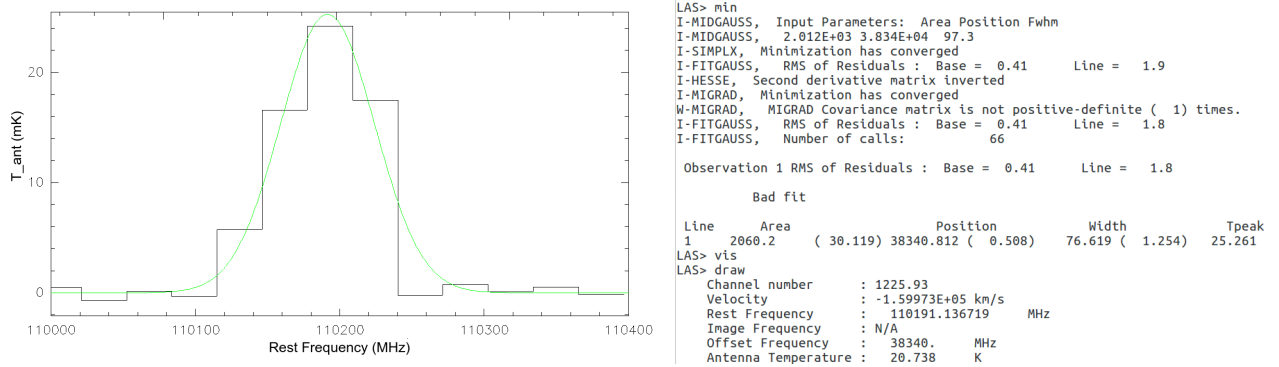


Figure 3.4: NGC 4414 spectrum between 75 and 111 GHz. All the detected species in the galaxy are indicated.



(a) A Gaussian fitted to a detected line.

(b) NGC 891 as example of an edge-on spiral galaxy¹².

Figure 3.5: Example of how CLASS package of GILDAS works.

	σ
	[km / s]
NGC 4826	44.78
NGC 2903	48.05
NGC 4414	45.22

Table 3.4: Selected σ value for each galaxy to calculate the upper limit of the area integral.

deviation (σ) was obtained by the equation 3.3:

$$FWHM = 2 \sqrt{2 \ln 2} \approx 2.35482\sigma, \quad (3.3)$$

the used FWHM values were collected from CLASS.

In this way, from equations 3.2 and 3.3, the integral of the Gaussian can be calculated using the equation 3.4:

$$I = T_{mbpeak} \left(\frac{FWHM}{2.35482} \right) \sqrt{2\pi}, \quad (3.4)$$

which have units of [K km s⁻¹]. The uncertainty related to the area integral will be calculated according to the method used by Turner (1991)⁴⁶ where the calculation is made for each point (detection) from the rms channel-to-channel noise and is given by equation 3.5:

$$\Delta I = m^{-1/2} \sigma, \quad (3.5)$$

where m is the number of channels of the line.

Upper Limit Estimation

Some molecular species were not detected in the three galaxies. For this reason, their upper limit of their line intensity was calculated assuming a limit in the area integral given by the equation 3.6:

$$I \leq 3 * rms * \sigma * \sqrt{2\pi}, \quad (3.6)$$

where rms is the signal to noise ratio (see Table 3.2), and σ value is the Gaussian parameters and was selected from the lowest sigma belonging to a line detected for each galaxy as shown in Table 3.4.

Finally, Tables 3.7, 3.7, and 3.7 show line parameters of the principal species observed in NGC 4826, NGC 2903, and NGC 4414 respectively. The parameters of the complex molecules were not calculated since to be sure of their detection it is suggested to carry out new observations.

Table 3.5: List of the molecular species identified in NGC 4826 with their respective line parameters.

Name	Frequency (GHz)	Transition	E ^a (s ⁻¹)	μ^b (Deb.)	T_{mb} Peak (K)	$\int T_{mb}dv$ (K km s ⁻¹)	FWHM (km s ⁻¹)
HC ₃ N	90.99272	10-9	5.813e-05	3.724	<1.02917e-03	<1.15512e-01	-
H ¹³ CN	86.33937	1-0	2.220e-05	2.980	2.57181e-03	6.76634e-01±0.11	247.16302
HN ¹³ C	87.09563	1-0	1.870e-05	2.700	4.16333e-04	7.67939e-02±0.12	173.28195
C ₂ H	87.33602	1-0	1.272e-06	0.800	3.72403e-03	1.457440±0.12	367.65931
HNCO	87.91816	4-3	6.310e-6	-	<1.02917e-03	<1.155123e-01	-
HCN	88.64126	1-0	2.400e-5	2.985	2.21458e-02	6.22937±0.12	264.25280
HCO ⁺	89.19686	1-0	4.200e-5	3.900	1.47111e-02	4.14910±0.11	264.95777
HNC	90.67778	1-0	2.700e-5	3.050	7.99153e-03	2.37635±0.12	279.34959
N ₂ H ⁺	93.18650	1-0	3.800e-5	4.400	3.15867e-03	8.93339e-01±0.07	265.69298
C ³⁴ S	96.38880	2-1	1.600e-05	1.957	6.14000e-04	9.71761e-02±0.08	148.68221
CS	97.98946	2-1	2.200e-05	1.957	6.73400e-03	1.94091±0.06	270.76994
C ¹⁸ O	109.79991	1-0	6.500e-8	0.111	5.90414e-03	1.67469±0.12	266.46744
¹³ CO	110.21991	1-0	6.500e-8	0.111	5.75229e-02	1.63966e+01±0.10	267.78193

^a Transition Energy.^b Dipole Moment

Table 3.6: List of the molecular species identified in NGC 2903 with their respective line parameters.

Name	Frequency (GHz)	Transition	E ^a (s ⁻¹)	μ^b (Deb.)	$T_{mb}Peak$ (K)	$\int T_{mb}dv$ (K km s ⁻¹)	FWHM (km s ⁻¹)
HC ₃ N	81.86906	9-8	4.215e-05	3.724	8.68918e-04	2.545175e-01±0.08	275.17354
H ¹³ CN	86.33937	1-0	2.220e-05	2.980	<8.75410e-04	<1.05434e-01	-
HN ¹³ C	87.09563	1-0	1.870e-05	2.700	<8.75410e-04	<1.05434e-01	-
C ₂ H	87.33102	1-0	1.272e-06	0.800	4.09410e-03	1.92274±0.18	441.19374
HNCO	87.91816	4-3	6.310e-6	-	1.78082e-03	2.75313e-01	145.23621
HCN	88.62754	1-0	2.400e-5	2.985	2.12705e-02	4.59157±0.18	202.79249
HCO ⁺	89.18353	1-0	4.200e-5	3.900	1.54993e-02	3.22647±0.18	195.56077
HNC	90.66437	1-0	2.700e-5	3.050	6.14951e-03	1.25266±0.09	191.36404
N ₂ H ⁺	93.16809	1-0	3.800e-5	4.400	2.55520e-03	5.68858e-01±0.06	209.14457
C ³⁴ S	96.41896	2-1	1.600e-05	1.957	4.98820e-04	7.03165e-02±0.06	132.42831
CS	97.98300	2-1	2.200e-5	1.957	3.69240e-03	8.76271e-01±0.05	222.94480
C ¹⁸ O	109.77408	1-0	6.500e-8	0.111	9.34967e-03	1.91923±0.11	192.84061
¹³ CO	110.19138	1-0	6.500e-8	0.111	4.21017e-02	9.34849±0.11	208.59798

^a Transition Energy.^b Dipole Moment

Table 3.7: List of the molecular species identified in NGC 4414 with their respective line parameters.

Name	Frequency (GHz)	Transition	E ^a (s ⁻¹)	μ^b (Deb.)	$T_{mb}Peak$ (K)	$\int T_{mb}dv$ (K km s ⁻¹)	FWHM (km s ⁻¹)
HC ₃ N	109.394234219	12-11	1.010e-04	3.724	1.97929e-03	2.85895e-01±0.15	135.69545
H ¹³ CN	86.33937	1-0	2.220e-05	2.980	<1.11250e-03	<1.26103e-01	-
HN ¹³ C	87.09563	1-0	1.870e-05	2.700	<1.11250e-03	<1.26103e-01	-
C ₂ H	87.34729	1-0	1.272e-06	0.800	1.95222e-03	1.30969±0.09	630.23935
HNCO	87.91816	4-3	6.310e-6		<1.11250e-03	<1.261025e-01	-
HCN	88.62908	1-0	2.400e-5	2.985	6.63847e-03	2.31207±0.11	327.19059
HCO ⁺	89.18943	1-0	4.200e-5	3.900	4.64097e-03	1.21832±0.13	246.61444
HNC	90.65392	1-0	2.700e-5	3.050	1.40375e-03	3.89148e-01±0.13	260.43111
N ₂ H ⁺	93.16430	1-0	3.800e-5	4.400	1.87850e-03	5.51689e-01±0.10	275.89968
C ³⁴ S	96.41896	2-1	1.600e-05	1.957	<1.16000e-03	<1.31487e-01	-
CS	97.98300	2-1	2.200e-5	1.957	<1.16000e-03	<1.31487e-01	-
C ¹⁸ O	109.76307	1-0	6.500e-8	0.111	3.61500e-03	1.23659±0.11	321.35397
¹³ CO	110.18267	1-0	6.500e-8	0.111	1.73057e-02	5.45942±0.10	296.36331

^a Transition Energy.^b Dipole Moment

Table 3.8: Detected molecular transitions for my galaxies.

Chemical formula	Transition	E_u^a (K)	A_{ij}^b (s^{-1})
$H^{13}CN$	1-0	4.14	2.22e-5
$HN^{13}C$	1-0	4.18	1.87e-5
C_2H	1-0	4.19	1.27e-6
HCN	1-0	4.25	2.40e-5
HCO^+	1-0	4.28	4.20e-5
HNC	1-0	4.35	2.70e-5
N_2H^+	1-0	4.47	3.80e-5
$C^{34}S$	2-1	6.25	1.60e-5
CS	2-1	7.05	2.20e-5
$C^{18}O$	1-0	5.27	6.50e-8
^{13}CO	1-0	5.29	6.50e-8

^a Energy of upper level above ground.

^b Einstein A coefficient.

3.3 Column Densities Estimation

The averaged column densities of the detected molecules were calculated by using the method described in Wilson et al (2013)⁴⁷. To develop this calculation, they used the equation 3.7:

$$N_l = 1.95 * 10^3 \frac{g_l \nu^2}{g_u A_{ul}} \int T_{mb} dV, \quad (3.7)$$

where N_l represent the column density in a level l and is in units of cm^{-2} , g_l and g_u are constants that can be calculated as $g_j = 2 * j + 1$ where j is the level of the particle, the subscript u corresponds to the *upper* level while the l to the *lower* level, ν is the frequency in units of GHz, A_{ul} is the Einstein A coefficient in units of s^{-1} , and T_{mb} is the main beam temperatures (The calculation of the error related to N_l is described in the appendix section A). Using this equation it is assumed that the lines emissions are optically thin and all the molecules in that column can be seen. In table 3.8 you can see a collection of Einstein A coefficients with some other essential parameters for some molecules.

The Boltzmann equation (Eq. 3.8) was used to calculate the total column density of each molecule:

$$N_{tot} = N_J \frac{Z}{2J + 1} e^{\frac{hBJ(J+1)}{kT_{ext}}}, \quad (3.8)$$

where N_J is the column density of the molecule at the J level, Z is the partition function, h is the Planck constant, B is the rotational constant, k is the Boltzmann constant, and T_{ext} is the excitation temperature that as we are in LTE

is the same for all transitions ($T_{ext} = 10$ K) (The calculation of the error related to N_{tot} is described in the appendix section A). This approximate value chosen for the excitation temperature is one of the strongest assumptions made in this work, and was chosen based on values used by other research groups (e.g. Watanabe et al. (2014)⁴⁸, Aladro et al. (2013)⁴⁹, Aladro et al. (2015)⁴, Nakajima et al. (2018)⁵⁰) that propose that it is the most suitable value for the study of this type of objects (dense molecular clouds). In addition, that excitation temperature was chosen because I want to compare the results obtained in this work with the aforementioned works.

Partition Function

The equation used to calculate the partition function Z will depend on whether the molecular species are linear, symmetric tops or asymmetric tops.

- Z was calculated for **linear species** applying the equation 3.9. The detected linear species detected in this work were ^{13}CO , $C^{18}O$, CS , $C^{34}S$, HCN , $H^{13}CN$, HCO^+ , HNC , N_2H^+ , and C_2H .

$$Z = \sum_{J=0}^{\infty} (2J + 1) * e^{-\left(\frac{hBJ(J+1)}{kT_{ext}}\right)}. \quad (3.9)$$

- Z for **symmetric tops species** was calculated using the equation 3.10. Symmetric specie detected in this work was CH_3CN .

$$Z = \frac{1}{3} \left[\frac{\pi(kT_{ext})}{h^3AB^2} \right]^{1/2}. \quad (3.10)$$

- Z for **asymmetric tops species** was calculated applying the equation 3.11. Asymmetric specie detected in this work was CH_3OH .

$$Z(A) = Z(E) = \left[\frac{\pi(kT_{ext})^3}{h^3ABC} \right]^{1/2}. \quad (3.11)$$

It is important to highlight that the partition function is the term with the greatest uncertainty in the calculation of the columnar density since again the approximation of a single excitation temperature of 10 K is used, which means that we are in LTE.

Upper Limit Estimation

In the case of the undetected lines, an upper limit of the average column density was calculated. That is, in the term $\int T_{mb}dV$ of equation 3.7 the upper limit of the line integral calculated in 3.2 was used. In the same way, the total columnar density was calculated from the upper limit of the average columnar density.

Finally, Table 3.9 shows the total column densities calculated for the three galaxies in my sample.

<i>Source averaged column densities [cm⁻²]</i>			
Molecule	NGC 4826	NGC 2903	NGC 4414
HC ₃ N	$< 6.94551 * 10^{11}$	$(1.206736 \pm 0.39) * 10^{12}$	$(3.334131 \pm 1.79) * 10^{12}$
H ¹³ CN	$(3.72510 \pm 0.98) * 10^{11}$	$< 5.80450 * 10^{10}$	$< 6.94238 * 10^{10}$
HN ¹³ C	$(5.09506 \pm 8.47) * 10^{10}$	$< 6.99524 * 10^{10}$	$< 8.36654 * 10^{10}$
C ₂ H	$(1.45457 \pm 0.26) * 10^{13}$	$(1.91873 \pm 0.25) * 10^{13}$	$(1.30744 \pm 0.22) * 10^{13}$
HCN	$(3.31304 \pm 0.40) * 10^{12}$	$(2.44124 \pm 0.30) * 10^{12}$	$(1.22932 \pm 0.18) * 10^{12}$
HCO ⁺	$(1.27500 \pm 0.16) * 10^{12}$	$(9.91184 \pm 1.29) * 10^{11}$	$(3.74321 \pm 0.78) * 10^{11}$
HNC	$(1.16535 \pm 0.18) * 10^{12}$	$(6.14114 \pm 1.08) * 10^{11}$	$(1.90735 \pm 0.84) * 10^{11}$
HNCO	$< 1.32162 * 10^{12}$	$(3.14997 \pm 1.23) * 10^{12}$	$< 1.44279 * 10^{12}$
N ₂ H ⁺	$(3.25109 \pm 0.60) * 10^{11}$	$(2.06940 \pm 0.44) * 10^{11}$	$(2.00678 \pm 0.58) * 10^{11}$
C ³⁴ S	$(2.24942 \pm 1.98) * 10^{11}$	$(1.62869 \pm 1.49) * 10^{11}$	$< 3.04554 * 10^{11}$
CS	$(3.50353 \pm 0.31) * 10^{12}$	$(1.58155 \pm 0.18) * 10^{12}$	$< 2.37315 * 10^{11}$
C ¹⁸ O	$(4.67325 \pm 0.90) * 10^{14}$	$(5.35313 \pm 0.96) * 10^{14}$	$(3.44840 \pm 0.73) * 10^{14}$
¹³ CO	$(4.59733 \pm 0.59) * 10^{15}$	$(2.61980 \pm 0.35) * 10^{15}$	$(1.52969 \pm 0.22) * 10^{15}$

Table 3.9: Total column densities calculated for the three galaxies NGC 4826, NGC 2903, NGC 4414.

3.4 Estimation of physical parameters of the molecular medium in my galaxies

An estimation of the physical parameters of the molecular gas of each galaxy can be obtained under the assumption of LTE and using different molecular isotopes. In my data, I detect several molecular isotopes like ¹³CO and C¹⁸O. The method assumes that one of the isotopes has to be optically thin (that is the optical depth of the line is $\tau \ll 1$), and the other one optically thick ($\tau > 1$). The optical depth is used to get an idea of how transparent or not a medium is for a given wavelength, this measurement is dimensionless. Generally the ¹²CO lines are optically thick due to the great abundance of this isotopes in molecular clouds, while the ¹³CO lines are generally optically thin²³. However, since we do not detect ¹²CO molecules in my data, we will work with other isotopes such as ¹³CO and C¹⁸O.

The solution of the transport equation at the center of the line is given by the equation 3.12:

$$T_L(0) = [\zeta(T_{ext}) - \zeta(T_{bg})] * (1 - e^{-\tau_0}), \quad (3.12)$$

where T_L is the maximum temperature of the transition line (in our case, it is T_{mb} the temperature calculated in section 2.3.2), T_{ext} is the excitation temperature, T_{bg} is the temperature of the cosmic background radiation (~ 2.73 K), τ_0 is the opacity, and ζ is defined in the equation 3.13:

$$\zeta(T) = \frac{hv/k}{e^{hv/kT} - 1}. \quad (3.13)$$

	T_{mb}^{13}	$T_{ext}^{J=1 \rightarrow 0}$
	[K]	[K]
NGC 4826	$5.75 \cdot 10^{-2}$	2.81
NGC 2903	$4.21 \cdot 10^{-2}$	2.79
NGC 4414	$1.73 \cdot 10^{-2}$	2.75

Table 3.10: Excitation Temperatures ($T_{ext}^{J=1 \rightarrow 0}$) of the ^{13}CO molecule of the three galaxies.

3.4.1 Excitation Temperature

In my case, since ^{13}CO is optically thick, the radiative transport equation (eq. 3.12) reduces to equation 3.14.

$$T_L^{13}(0) = [\zeta^{13}(T_{ext}) - \zeta^{13}(T_{bg})]. \quad (3.14)$$

From equation 3.14, the excitation temperature (T_{ext}) can be solved by obtaining equation 3.15.

$$T_{ext} = T_K = \frac{h\nu/k}{\ln \left[1 + \frac{h\nu/k}{T_L^{13}(0) + \zeta^{13}(2.73K)} \right]}, \quad (3.15)$$

$$\Rightarrow T_{ext}^{J=1 \rightarrow 0} = T_K = \frac{5.29}{\ln \left[1 + \frac{5.29}{T_L^{13}(J=1 \rightarrow 0)(0) + 0.89} \right]}. \quad (3.16)$$

Now, using equation 3.16 the excitation temperature of the ^{13}CO molecule of the three galaxies was calculated, and the results are shown in Table 3.10.

3.4.2 Optical Depth

To calculate the optical depth, it must be assumed that the excitation temperature (T_{ext}) is the same for all the isotopic species of a molecule, that is, everything is thermalized: $T_{ext}(^{13}CO) = T_{ext}(C^{18}O) = T_K$. In this way, from the observed line of ^{13}CO , its optical depth can be calculated using the radial transport equation (3.12), obtaining the equation 3.17, where the superscript 13 represents the isotope which in this case is ^{13}CO .

$$T_L^{13}(0) = [\zeta^{13}(T_{ext}) - \zeta^{13}(T_{bg})] * (1 - e^{-\tau_0^{13}}). \quad (3.17)$$

Equation 3.14 can be solved for opacity or optical depth resulting in the equation

$$\tau_0^{13} = -\ln \left[1 - \frac{T_L^{13}(0)}{\zeta^{13}(T_{ext}) - \zeta^{13}(T_{bg})} \right]. \quad (3.18)$$

Another way to obtain τ_0^{13} is from the quotient of intensities between isotopes. For instance, the quotient between the lines of the same transition of two isotopic varieties such as ^{13}CO and $C^{18}O$ which resulting in the equation 3.19.

Table 3.11: Detected molecular transitions for my galaxies.

Source	$T_L^{12}(0)$ ^a (K)	$T_L^{18}(0)$ (K)	τ_0^{18}
NGC 4826	0.64	0.90e-3	1.41e-3
NGC 2903	2.67	9.35e-3	3.51e-3
NGC 4414	0.64	3.62e-3	5.67e-3

^a Nakajima et al. (2018)⁵⁰.

$$\frac{T_L^{18}(0)}{T_L^{13}(0)} = \frac{\zeta^{18}(T_{ext}) - \zeta^{18}(T_{bg})}{\zeta^{13}(T_{ext}) - \zeta^{13}(T_{bg})} (1 - e^{-\tau_0^{18}}) \approx 1 - e^{-\tau_0^{18}}. \quad (3.19)$$

However, due to ^{13}CO is optically thin, Eq. 3.19 cannot be used for calculating optical depth. For this reason, the ^{12}CO molecule, which is known to be typically optically thick, was used for the calculation of optical depth. As ^{12}CO was not detected in any of the galaxies in my sample, I used typical temperature values for galaxies similar to mine with the same nuclear activity. In this way, Eq. 3.19 is rewritten as:

$$\frac{T_L^{18}(0)}{T_L^{12}(0)} = \frac{\zeta^{18}(T_{ext}) - \zeta^{18}(T_{bg})}{\zeta^{12}(T_{ext}) - \zeta^{12}(T_{bg})} (1 - e^{-\tau_0^{18}}) \approx 1 - e^{-\tau_0^{18}}, \quad (3.20)$$

$$\implies \tau_0^{18} \approx -\ln \left(1 - \frac{T_L^{18}(0)}{T_L^{12}(0)} \right). \quad (3.21)$$

Using equation 3.21, the opacity was calculated for $C^{18}O$ molecules of the three galaxies obtaining that in the three galaxies this molecule is optically thin, as shown in Table 3.11.

3.4.3 H_2 Column Density

If the relative abundance between H_2 and $C^{18}O$ is known, the column density of H_2 can be easily calculated from the column density of $C^{18}O$ ⁵. The relationship that is usually adopted is⁵¹:

$$\frac{N(C^{18}O)}{N(H_2)} \approx 2 * 10^{-7}, \quad (3.22)$$

$$\implies N(H_2) = 5 * 10^6 N(C^{18}O). \quad (3.23)$$

Table 3.12 shows the column density of H_2 calculated for the three galaxies in my sample.

	$N(C^{18}O)$ (cm^{-2})	$N(H_2)$ (cm^{-2})
NGC 4826	$4.67 \cdot 10^{14}$	$2.34 \cdot 10^{21}$
NGC 2903	$5.35 \cdot 10^{14}$	$2.68 \cdot 10^{21}$
NGC 4414	$3.45 \cdot 10^{14}$	$1.38 \cdot 10^{21}$

Table 3.12: Column density of H_2 calculated for the three galaxies.

Chapter 4

Analysis & Discussion of Results

In this chapter, the detected lines and the calculated abundances will be analyzed and compared to know what the environment of the molecular clouds of the galaxies in my sample is like, and to know if there are similarities with “typical” galaxies in the literature whose nuclear activity is similar. For this, first the detection of the molecules of each galaxy will be compared to see if there are molecules characteristic of AGNs and Starburst. Subsequently, the calculated abundances will be compared between AGNs and Starburst since it would be expected that depending on the nuclear activity of the galaxies, the formation of certain molecules is favored.

4.1 Comparison between the spectra of the galaxies

First, I made a visual comparison between the reduced spectra of the three galaxies, and for a better comparison the spectra were normalized to two different molecules: ^{13}CO and HCN . The normalization with respect to ^{13}CO was carried out because it is the most intense line detected in the three galaxies, also the CO molecule (or in this case its ^{13}CO isotope) is the most important for the generalized study of molecular clouds. This is because the characteristics of this molecule make it suitable for the study of IM⁵. On the other hand, the normalization of the spectra with respect to the HCN molecule was also carried out, since its identification and abundance are classified as good discriminators between types of environments and galaxies⁴. Furthermore, the ^{13}CO molecule gives information about the total gas in the molecular cloud, while the HCN molecule gives information about the dense gas which is directly related to the star formation. Since it is not yet known with certainty if it is the total gas or only the dense gas that has the greatest influence on star formation, both cases must be analyzed. Figures 4.2 and 4.3 show this normalization with respect to ^{13}CO and HCN molecules respectively. In both figures the most intense molecules were labeled as they are good candidates to make a discrimination or distinction between AGNs and Starburst type galaxies.

To see if the spectrum of my galaxies have any trend or discrimination between AGNs and Starburst, the spectra obtained by Aladro et al. (2015)⁴ will be used since they belong to a larger sample with a total of eight galaxies of different nuclear activity, which are shown in Figure 4.1. This figure shows the galaxies ordered according to their

star formation rate and nuclear activity, with M83 (Young Starburst) being the galaxy with the least star formation rate, and Mrk231 (Ultra-luminous infrared galaxy (ULIRG)) the galaxy with the greatest star formation rate.

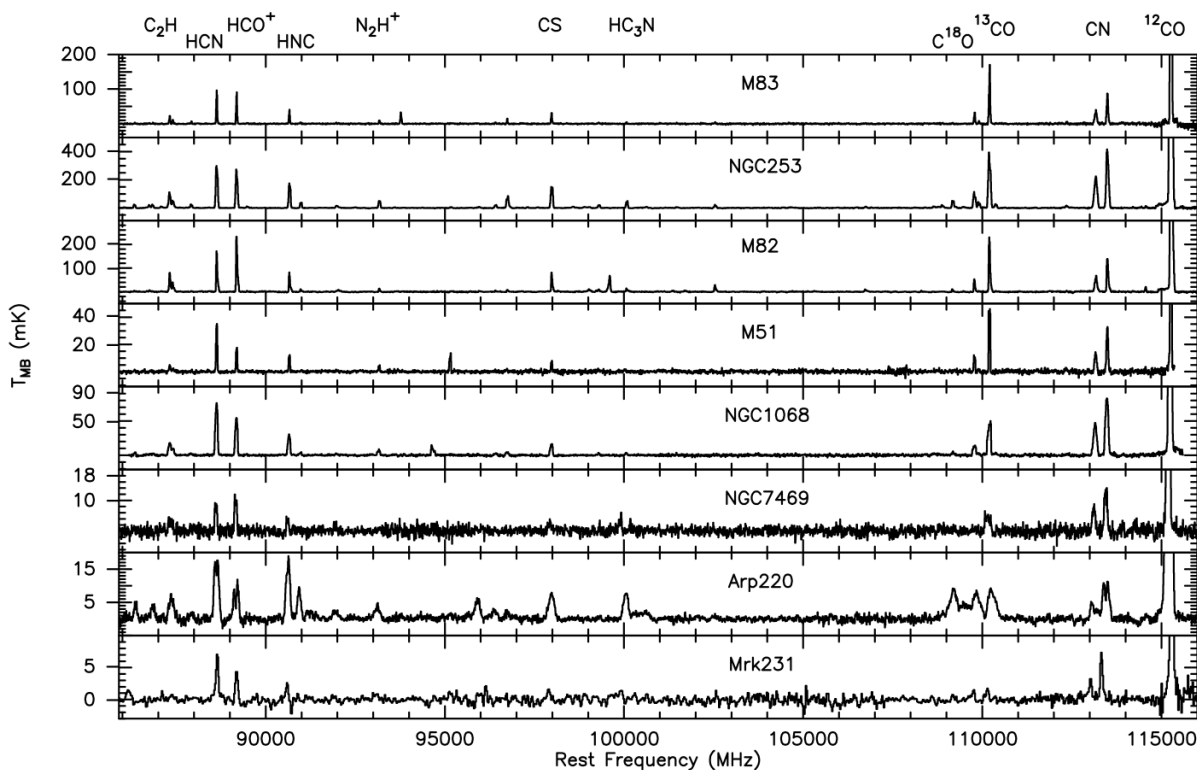


Figure 4.1: Spectra of eight galaxies taken from Aladro et al. (2015)⁴.

At first glance, it can be seen that in the three galaxies of my sample the predominant line belong to the ^{13}CO molecule which is a typical phenomenon in spiral galaxies or with small star formation, as can be seen in Figure 4.1. In the same way, the ratio of ^{13}CO and HCN seems to vary with the nuclear activity of the galaxy since the higher this activity, the HCN molecule begins to predominate instead of ^{13}CO . The relationship between ^{13}CO and C^{18}O tends to be unity as the nuclear activity increases. Likewise, it appears that the intensity of HNC increases with the rate of star formation, so does it. Finally, it appears that the intensity of the CS molecule also increases as nuclear activity increases. These are the main characteristics that can be extracted from the study by Aladro et al. Now, it seeks to find if the galaxies in my sample have the same trend.

Studying Figure 4.2, it can be clearly seen that the HCN molecule in NGC 2903 is more intense compared to NGC 4414 and NGC 4826. This also happens with the HCO^+ molecule. At first glance, it could be said that the intensity of these molecules in relation to the total gas of the molecular cloud is a possible discriminator between Starburst and AGNs which agrees with the work of Aladro et al. specifically with NGC 253. In the Starburst galaxy, the HCN and HCO^+ molecules are more intense with approximate fractional intensities of 0.55 and 0.40 respectively.

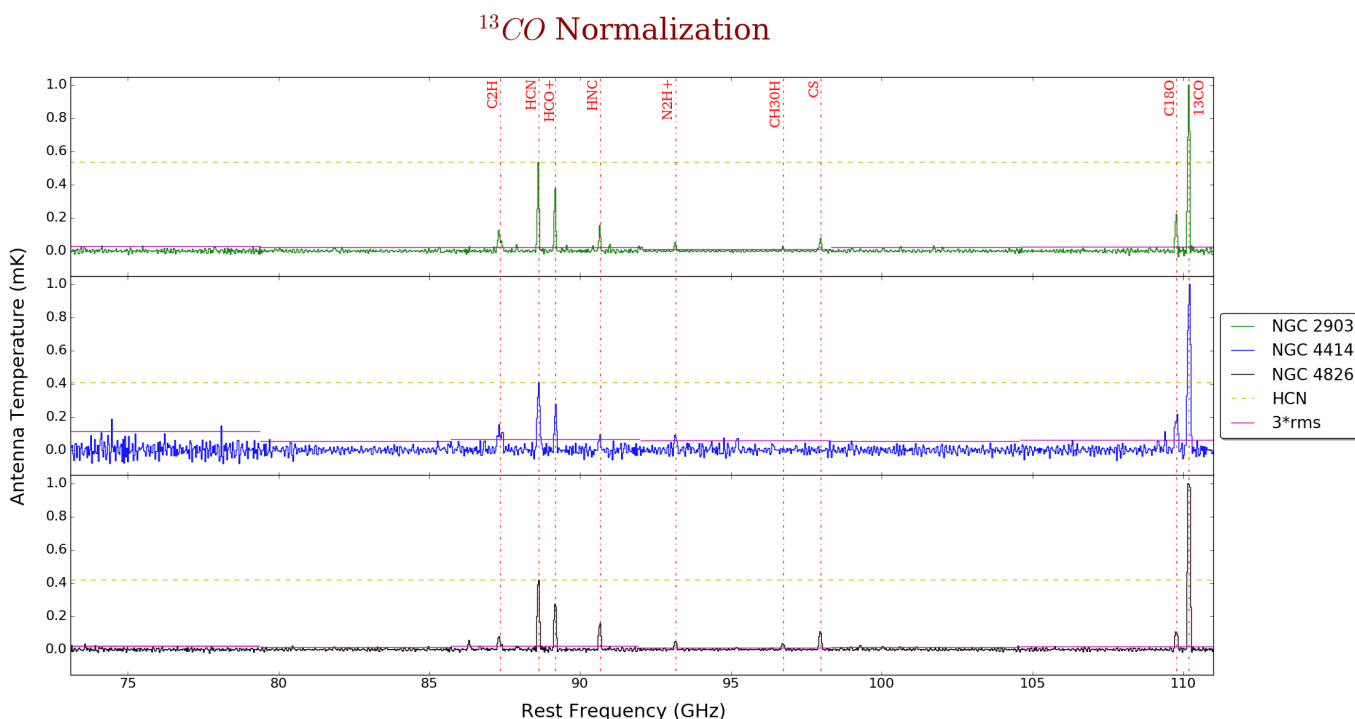


Figure 4.2: Spectra of three galaxies between 75 and 111 GHz normalized with respect to the ^{13}CO molecule.

On the other hand, the CS molecule in NGC 4826 is more intense than in NGC 2903. Since this molecule was not detected in NGC 4414, it could be said that this molecule is also a possible candidate to differentiate an AGN from a Starburst. Finally, C_2H in NGC 4826 appear to be the weakest even though they were detected in the three galaxies.

Now, if we look at Figure 4.3, we can see that the ^{13}CO molecule is more intense in AGNs (NGC 4414 and NGC 4826) than in Starburst (NGC 2903), that is, when we study only dense gas ^{13}CO is more predominant in AGNs. The C_2H molecule is more intense in NGC 4414 than in NGC 4826 and NGC 2903 but this may be because NGC 4414 has a high noise. This also happens with the molecule of N_2H^+ and C^{18}O . Although HNC was detected in all three galaxies, it is most intense in NGC 4826. For the CS molecule, the same happens as the previous case, it was only detected in NGC 2903 and NGC 4826, being more intense in the second one. In this case, when we normalized the spectra with respect to the HCN molecule, the molecule that appear to be invariant of the nuclear activity of galaxies is HCO^+ .

In this way we can realize that depending on whether we study the total gas of the molecular cloud or if we only consider the dense gas, the emission of one or another molecule will be more intense than another. However, when we study the total gas of the molecular clouds of the galaxies in my sample, it coincides with what is found in the literature.

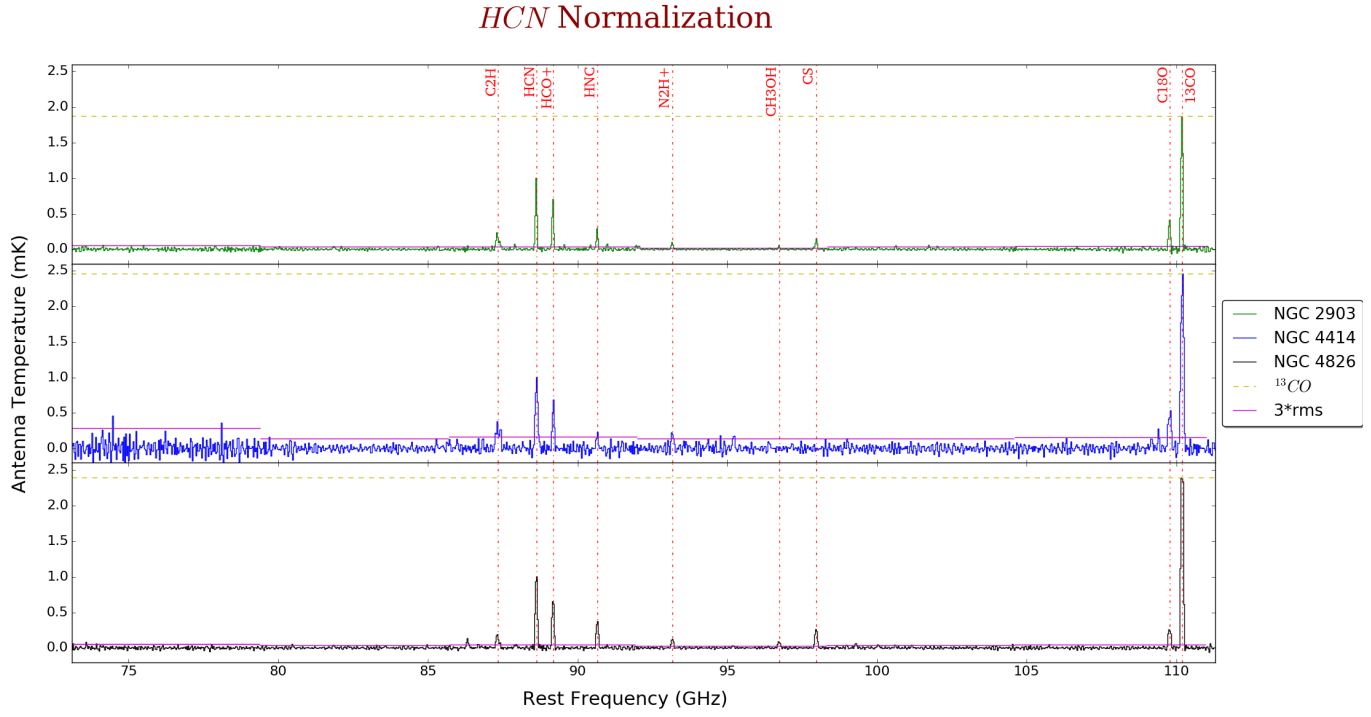


Figure 4.3: Spectra of three galaxies between 75 and 111 GHz normalized with respect to the *HCN* molecule.

4.1.1 Line Ratios

As mentioned in 2.1, reports of the integrated intensity of a few molecules of the galaxies studied in this work were found in the literature. In this section we will compare what we obtained with the literature to check the consistency of our results. Table 4.1 shows this comparison.

As we can see, the intensity calculated in this work coincide with those found in the literature, which confirms the veracity of its development. The only intensity that varies is the one that belongs to I_{1-0}^{13CO} in NGC 2903. The main reason for this inconsistency is the instrument with which the two observations were made. Vila-Vilaro et al.(2015)³⁵ made the observations with the ARO 12 m telescope, while my observations were with the LMT 32 m telescope. This means, that I am looking at a larger area of the galaxy (nucleus plus part of the galaxy itself), while Vila-Vilaro et al. is concentrating only on its center. With this result, it could be said that tentatively in NGC 2903 the intensity of the 13CO (1-0) line comes from the center of the galaxy, and in my observation it is diluted. For this reason, my intensity is greater than the one of Vila-Vilaro et al. (2015)

Table 4.1: Comparison between the integrated intensities obtained in this work with those found in the literature.

Source	I_{1-0}^{13CO} (K * km/s)		I_{1-0}^{HCN} (K * km/s)		$I_{1-0}^{HCO^+}$ (K * km/s)	
	NGC 2903	9.35±0.11 ^a	2.01±0.11 ^b	4.59±0.18 ^a	3.21±0.65 ^d	-
NGC 4826	-	-	6.23±0.12 ^a	6.0±0.4 ^c	4.15±0.11 ^a	3.5±0.1 ^c

^a Results of this work.

^b Vila-Vilaro et al.(2015)³⁵, observations made with Arizona Radio Observatory (ARO) 12 m telescope.

^c Krips et al. (2008)⁵², observations made with Institut de Radioastronomie Milimétrique (IRAM) 30 m telescope.

^d Topal (2018)³⁴, observations made with Berkeley-Illinois-Maryland Association (BIMA) telescope array and National Radio Astronomy Observatory (NRAO) telescope.

4.2 Comparison between the abundances of the galaxies

For this comparison, I perform a mixture between a visual comparison and an empirical one. Mathematically the ratios of the molecular abundances with respect to $C^{18}O$ and HCN molecules were calculated. Then, for a better study, these ratios were plotted and compared with the ratios of molecular abundances of other galaxies of our sample or galaxies from the literature. Due to the fact that there is no previous literature where the molecules of the galaxies studied in this work are detected and their abundances calculated, the comparison of the galaxies in our sample will be made with “typical” galaxies whose nuclear activity is similar. For instance, NGC 4826 and NGC 4414 (AGNs) from our sample will be compared with NGC 1068 and NGC 7469 (AGNs) studied by Aladro et al. (2015)⁴, and also with the work of Nakajima et al (2018)⁵⁰ who also studied NGC 1068 because it is considered as a “typical” AGN. On the other hand, NGC 2903 (Starburst) from our sample is compared with M82, M83 and NGC 253 (Starburst galaxies) from Aladro et al. (2015), as well as IC 342 from Nakajima’s et al (2018) work.

4.2.1 Molecules

The comparison of molecular abundances among these three galaxies is shown in Figure 4.4. An analysis and interpretation of the molecular abundances of the most relevant molecules of each galaxy will be carried out below.

- **^{13}CO and $C^{18}O$.**- There are some previous observations on ^{13}CO and $C^{18}O$ for NGC 4826 and NGC 2903. However, these observations only reported the integrated intensity and did not calculate the abundances. In our sample these two molecules were identified and they are the most intense and abundant. If we compare the abundance of these molecules among the three galaxies in my sample, it is evident that the N_{rot} of ^{13}CO in NGC 4826 is greater than in NGC 4414 and NGC 2903 by a factor of ~ 3 and ~ 1.75 respectively. On the

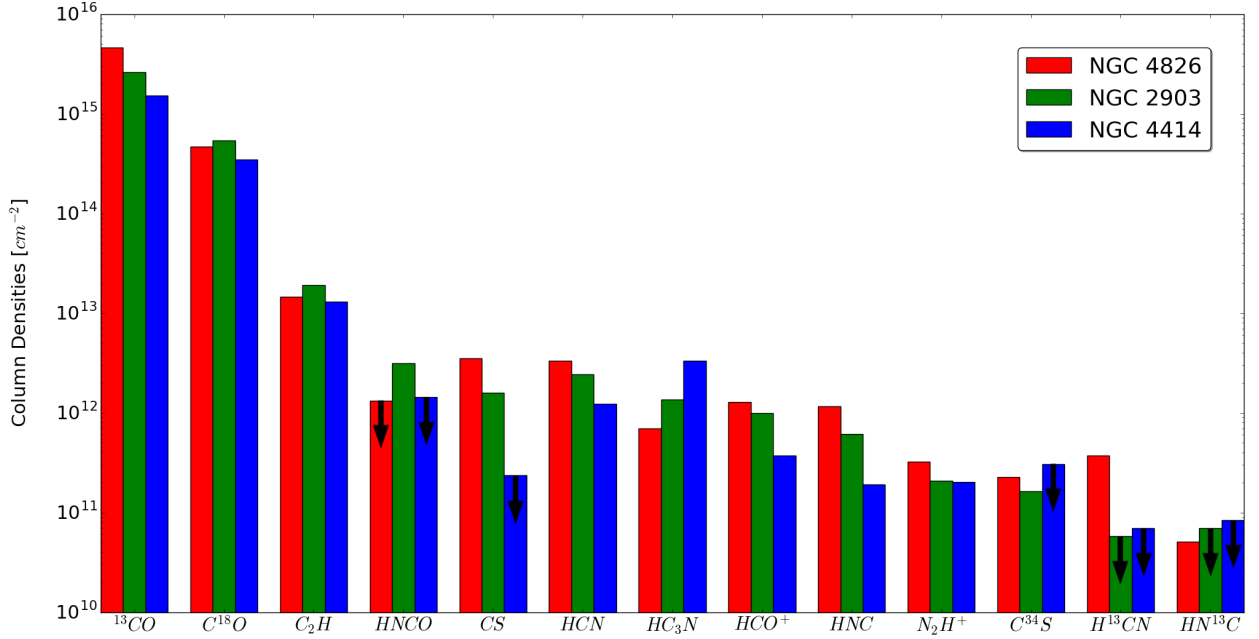


Figure 4.4: Comparison between the column densities of the galaxies. Black arrows indicate upper limit abundance.

other hand, the N_{tot} of C^{18}O in NGC 2903 is higher than in NGC 4826 and NGC 4414 by a factor of ~ 1.15 and ~ 1.55 respectively. However, if we make the comparison with typical AGNs and Starburst galaxies such as NGC 1068 and M82 respectively which were studied by Aladro et al. (2015)⁴, the abundances of ^{13}CO and C^{18}O are higher than ours with at least two orders of magnitude. Probably, this is due to the fact that the star formation rates of NGC 1068 and M82 are higher than the galaxies in our sample ($\sim 100\text{M}_{\odot}\text{yr}^{-1}$ for NGC 1068⁵³ and $\sim 10\text{M}_{\odot}\text{yr}^{-1}$ for M82⁵⁴). Finally, an interesting point that can be evidenced in these molecules is that all the isotropic molecules that contain ^{13}C are more abundant in NGC 4826 than in the other two galaxies. Henkel et al. (2014)⁵⁵ mentions that in massive stars ^{12}C molecule is predominantly synthesized, while in longer lived lower mass stars at later times the ^{13}C molecule is mostly ejected. From this information, it can be said that tentatively the last star formation outbreak or starburst of NGC 4826 occurred longer compared to the other galaxies, that is, it is a more evolved starburst, and therefore the stars that formed in it have aged more and are producing ^{13}C .

- **CS and C^{34}S .**- The two molecules were detected in NGC 4826 and NGC 2903 being more abundant in NGC 4826. N_{tot} of CS and C^{34}S in NGC 4826 is greater than in NGC 2903 by a factor of ~ 2.22 and ~ 1.38 respectively. This result may be an indicator that these molecules are probably more abundant in AGNs than in Starburst. This result is consistent with what Aladro et al. (2015)⁴ obtained since the abundances of CS and C^{34}S in NGC 1068 ($(7.6 \pm 0.2) \times 10^{14}\text{cm}^{-2}$ and $(1.3 \pm 0.2) \times 10^{14}\text{cm}^{-2}$) are also greater than in M82 ($(2.50 \pm 0.05) \times 10^{14}\text{cm}^{-2}$ and $(1.50 \pm 0.08) \times 10^{13}\text{cm}^{-2}$).

- **C₂H.**- It has been found in previous observational studies that this molecule has high abundances in Photon-dominated region (PDR)s of Starburst galaxies (e.g. Meier & Turner (2005)⁵⁶). This molecule was detected in the three galaxies of our sample, being more abundant in NGC 2903 by a factor of ~ 1.32 and ~ 1.47 for NGC 4826 and NGC 4414 respectively. This phenomenon is also evident in Aladro's et al. (2005)⁴ work since they reported that the abundance of this molecule in M 82 (typical Starburst) is greater than M 51 (Seyfert 2-type galaxy) by a factor of 5.
- **HCN, HCO⁺, and their ¹³C isotopic species.**- Model predictions (e.g. Lepp & Dalgarno (1996)⁵⁷; Meijerink & Spaans (2005)²⁶) and previous observations (e.g. Aalto (2008)⁵⁸) indicate that the HCN molecule can be produced in regions that are dominated by UV and X-ray fields, so this is expected to happen in Starburst galaxies and AGNs. This is evident in our sample since *HCN* and *HCO⁺* were detected in the three galaxies. We obtained values for N_{tot} of *HCN* ($(3.31304 \pm 0.40) * 10^{12} \text{cm}^{-2}$) in NGC 4826 which is approximately ~ 1.36 times higher than in the Starburst galaxy (NGC 2903). Nakajima et al. (2018)⁵⁰ reported a similar phenomenon where the calculated *HCN* abundance for NGC 1068 was 2-4 times greater than Starburst-like galaxies. Besides, the intensity ratios between *HCN* and *HCO⁺* are usually higher in AGNs than in Starburst (e.g. Kohno et al. (2008)⁵⁹), so it is a good discriminator between these two types of nuclear activity. On the other hand, *H¹³CN* was only detected in NGC 4826. However, it can be compared with the upper limit calculated for NGC 2903 which is lower than that obtained in NGC 4826. This agrees with what Nakajima obtained since they also reported that *H¹³CN* in NGC 1068 is > 3 times higher than in the Starburst galaxies.
- **HNC.**- It has been suggested that the influence of X-rays in X-ray dominated region (XDR) and/or UV radiation in PDRs are one of the causes of a bright HNC emission at densities $n \lesssim 10^4 \text{cm}^{-3}$ (e.g. Meijerink & Spaans (2005)²⁶). This phenomenon is expected to occur in AGNs and Starburst galaxies (e.g. Aladro et al. (2015)⁴). In our results, the N_{tot} of *HNC* in NGC 4826, $(1.16535 \pm 0.18) * 10^{12} \text{cm}^{-2}$, is approximately two times higher than those in the Starburst galaxy which is $(6.14114 \pm 1.08) * 10^{11} \text{cm}^{-2}$ in NGC 2903. Probably, the reason for this relative difference in abundances may be due to the strong emission that takes place in the galactic Circumnuclear disk (CND) in the AGN. Nakajima et al. (2018)⁵⁰ reported that the N_{tot} of *HNC* in NGC 1068 (AGN) is approximately two times higher than in NGC 253 and IC 342 (two Starburst galaxies), which it is consistent with our results.
- **N₂H⁺.**- This molecule is well know as a cold dense gas tracer (e.g. Bergin et al. (2002)⁶⁰). Nakajima et al. (2018)⁵⁰ mentioned that this molecule has been observed several times in Galactic molecular clouds. However, its observation in external galaxies, especially in AGNs, has been very limited. In our sample, *N₂H⁺* has been detected in the three galaxies, being more abundant in NGC 4826. If we compare this AGN with the Starburst, it is noted that the N_{tot} of *N₂H⁺* is approximately ~ 1.57 times more abundant. Nakajima et al. reported that the abundance of this molecule is 1.7-1.9 times higher in NGC 1068 than in those Starburst-like galaxies, which is consistent with our results.
- **HNCO.**- Aladro et al. (2015)⁴ mentions that this molecule in Starburst galaxies is a good indicator of its nuclear evolution since its abundance is diminished in the last evolutionary stages of this type of galaxies. In

our observations, the only galaxy in which this molecule was detected was in NGC 2903, the Starburst galaxy of our sample. If we compare our galaxy with a typical Starburst, such as M82 studied by Aladro et al., we can see that the abundance we obtained is at least one order of magnitude less than that obtained by Aladro.

As mentioned before, the abundances obtained in this work are at least one or two orders of magnitude smaller than the typical AGNs and Starburst galaxies that were studied by Aladro et al. (2015)⁴ and Nakajima et al. (2018)⁵⁰, and that were used for the comparison and development of this work. Probably, the main reason for this event could be that the star formation rate of the galaxies in our sample is lower than the galaxies used for the comparison. However, when we compare the abundances between the galaxies in our own sample, we find a concordance with the work done by Aladro et al. and Nakajima et al.. This may be a good indication that our galaxies have behaviors of typical AGNs and Starburst galaxies cited in the literature.

4.2.2 Abundance Ratios

Once the general study of the obtained abundances from each galaxy in our sample has been carried out, we will study what is the relationship that these abundances have with respect to the total gas and the dense gas of the molecular cloud. For this, the ratios of these abundances with respect to the abundances of the $C^{18}O$ and HCN molecules were calculated since they are related to total gas and dense gas respectively, as mentioned in 4.1, and which will be discussed below. Figures 4.5 and 4.6 show the comparison between the abundances normalized with respect to $C^{18}O$ and HCN respectively. For this comparison, we decided to use the $C^{18}O$ molecule since it is less affected by the opacity in comparison with the main oxygen isotopologue ^{13}CO (see Table 3.11).

When we study figure 4.5, we can realize that when doing the normalization with respect to $C^{18}O$ some of the abundances changed, which will be studied below:

- **$HNCO$.**- This molecule was only detected in NGC 2903. Due to $HNCO$ is a shock tracer, it indicates that this galaxy is probably forming molecular species in large numbers, which is to be expected in a Starburst galaxy.
- **HC_3N .**- The column density of this molecule appears to be significantly higher in NGC 4414 than in the other galaxies. HC_3N is especially found in hot and dense gas areas.
- **N_2H^+ .**- Aladro et al. reported that the AGNs studied in their work had a higher amount of $N_2H^+/C^{18}O$. This same trend is seen in my sample.
- **$C^{34}S$.**- Although this molecule was not detected in NGC 4414, it tends to be more abundant in AGNs when the total gas of the molecular cloud is studied.

On the other hand, when we study Figure 4.6 it seems that the abundances of the molecules compared between the three galaxies do not vary that much. This is an interesting conclusion since it can probably be indicated that what differentiates an AGN from a Starburst is not only its dense gas, but that all the gas in the molecular cloud gives specific characteristics to one or another type of nuclear activity.

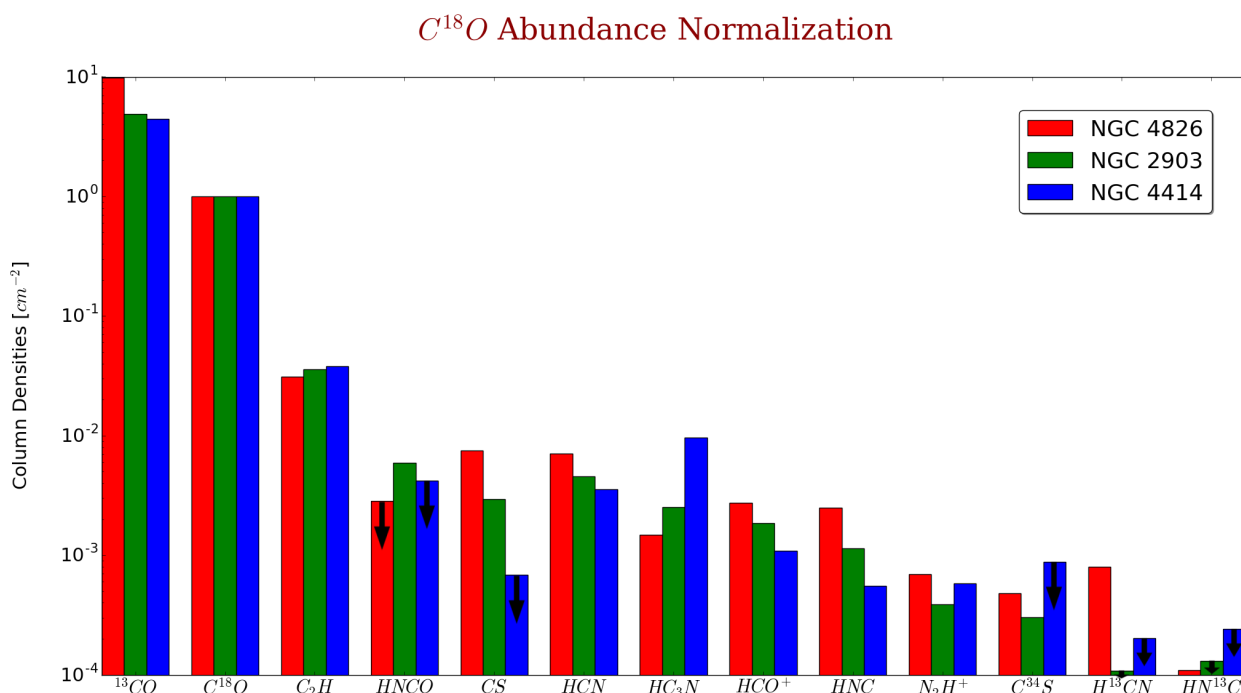


Figure 4.5: Comparison between the column densities of the galaxies normalized with respect to $C^{18}O$ abundance.

Finally, the last method used for the discussion was to compare by means of a plot the molecular abundances of each galaxies studied with typical galaxies classified as AGNs and Starburst. Figures 4.7 and 4.8 show this comparison normalized to $C^{18}O$ molecule.

In Figure 4.7, the Starburst galaxy of our sample is compared with three “typical” galaxies studied by Aladro et al. (2015)⁴, such as M83, NGC 253, and M82. The first one is an example of a young or early Starburst stage (e.g. Martín et al. 2009a⁶¹), the second is an intermediate Starburst stage, and the third is evolved or late Starburst one. In this way, the main objective of this comparison is to find the galaxy with which NGC 2903 shares the greatest characteristics in terms of molecular abundances, so in this way its evolutionary state can be known. This figure shows the molecules whose abundance was calculated in section 3.3 (see Table 3.9), if a molecule is not found in the plot it is because it was not detected in one of the two galaxies that are being compared. Making the comparison, we can realize that the galaxy whose abundances coincide more with the abundances calculated for NGC 2903 is M83. The molecules whose abundances coincide in the two galaxies are ^{13}CO and $C^{18}O$. The molecules whose abundances are higher in NGC 2903 are $C^{34}S$, N_2H^+ , HNC , HCO^+ , CS , HCN , and C_2H . The molecules whose abundances are greater in M83 are HC_3N and $HNCO$. From this result, we can state that NGC 2903 tentatively is a intermediate stage Starburst, as M83, with the difference that NGC 2903 has regions that are more dominated by UV and X-ray fields since its abundance of HCN , HCO^+ , and HNC is greater.

As in the previous case, in figure 4.8 we can see the comparison of the abundances obtained for NGC 4826 and

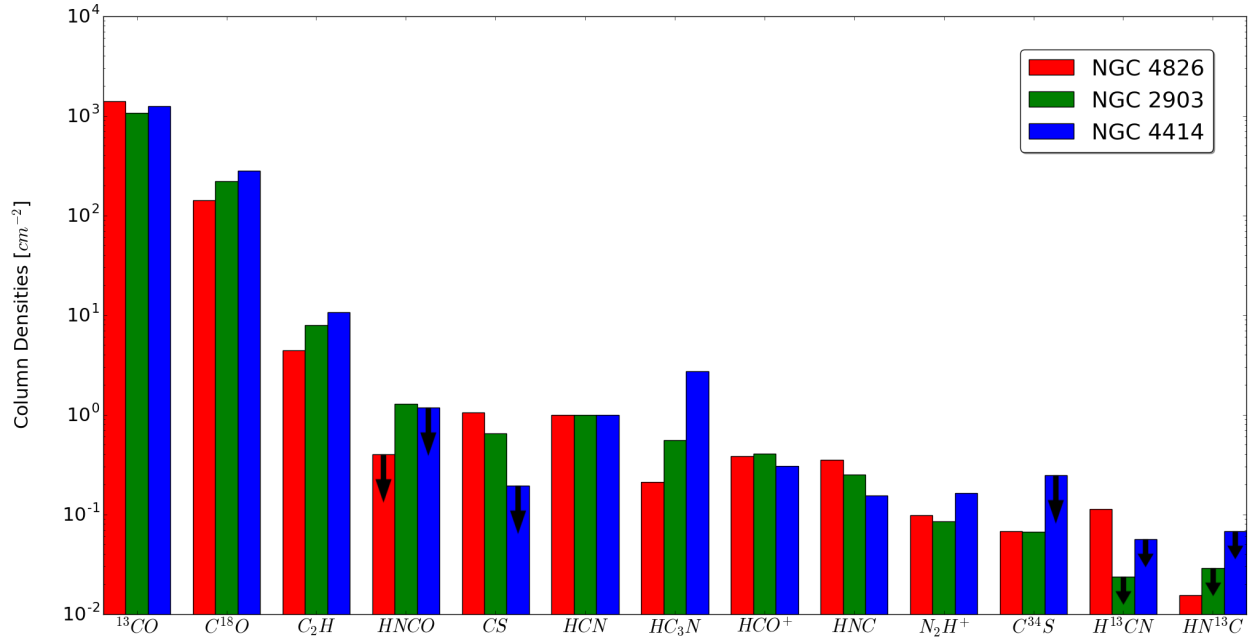
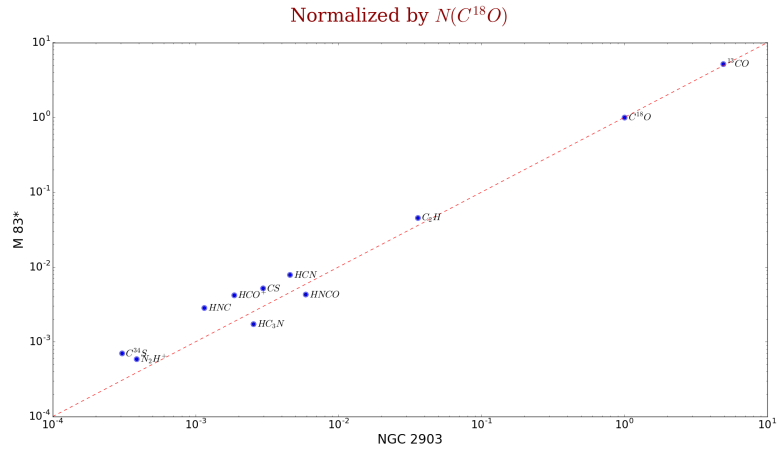
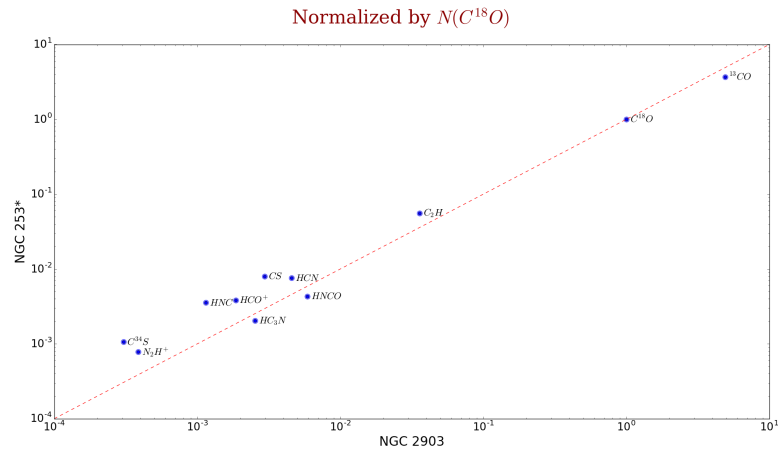
HCN Abundance Normalization

Figure 4.6: Comparison between the column densities of the galaxies normalized with respect to *HCN* abundance.

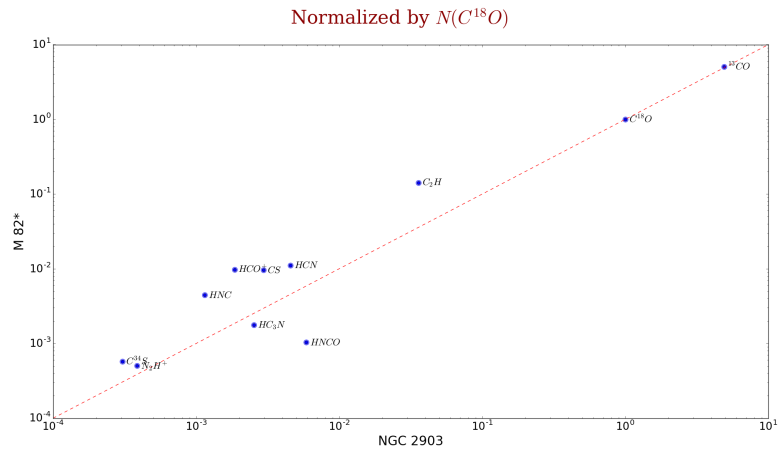
NGC 4414 with “typical” AGNs such as NGC 1068 (classified as type 2 Seyfert) and NGC 7469 (classified as type 1 Seyfert). First, the comparison between the two AGNs of our sample was made which is shown in Figure 4.8e. Here we can see that the comparison of the galaxies was only made with seven molecules since most were not detected in NGC 4414 due to its high rms on its spectrum. On the other hand, NGC 4826 and NGC 4414 were compared separately with each “typical” AGNs in order to confirm their classification since in section 2.1 we mentioned that the two galaxies are classified as type 2 Seyfert galaxies. In this way, we can realize that the abundances calculated for NGC 4826 are more similar to the abundances of NGC 1068 especially due to the number of detected molecules that they share. Similarly, the abundances of NGC 4414 are more similar to NGC 1068, which was to be expected.



(a) NGC 2903 vs M83. The M83 data for comparison were taken from Aladro (2015)⁴.



(b) NGC 2903 vs NGC 253. The NGC 253 data for comparison were taken from Aladro (2015)⁴.



(c) NGC 2903 vs M82. The M82 data for comparison were taken from Aladro (2015)⁴.

Figure 4.7: Plots of the fractional molecular abundances relative to $C^{18}O$. These results represent the abundance correlation between NGC 2903 with a typical Starburst galaxy. The red dashed lines represents equal abundances between the galaxies.

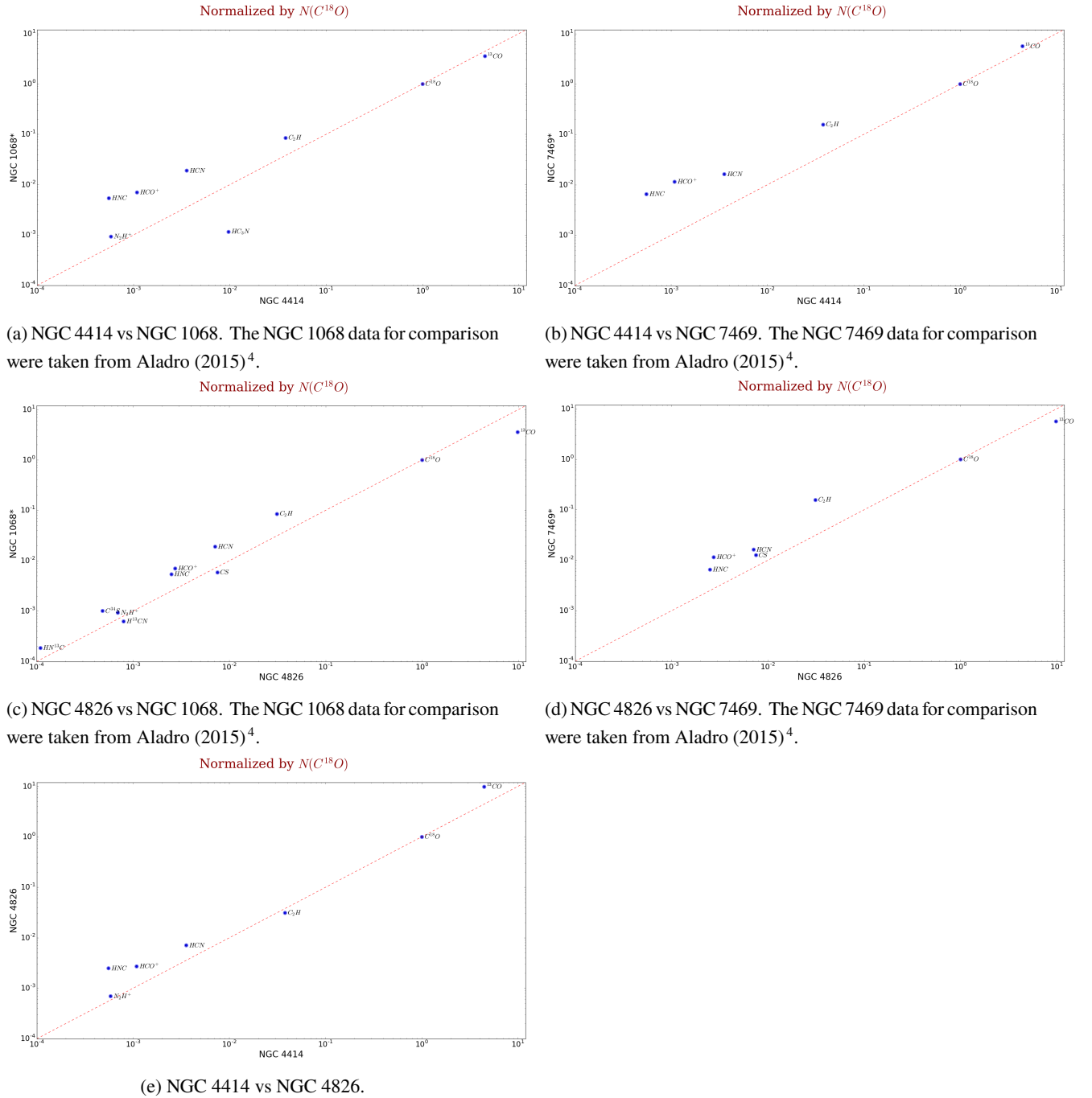


Figure 4.8: Plots of the fractional molecular abundances relative to $C^{18}O$. These results represent the abundance correlation between NGC 4414 and NGC 4826 with a typical AGN. The red dashed lines represents equal abundances between the galaxies.

Chapter 5

Conclusions

5.1 Conclusions

We presented a 3mm band observations in a frequency range $\sim [73 - 111]$ GHz towards three nearby galaxies, including NGC 2903, NGC 4826 and NGC 4414. The observations were made with the RSR on the 32 m LMT telescope at Mexico on different dates for each galaxy. The three galaxies share similar characteristics, the only main difference between them is their nuclear activity since NGC 4826 and NGC 4414 are AGNs, NGC 2903 is an Starburst type galaxy. The main objective of this work is to identify molecules that help differentiate between the two types of nuclear activity. For this, we studied the dense gas of the aforementioned galaxies. The procedure was as follows. First, I identified twenty three molecular species in NGC 4826, twenty eight molecular species in NGC 2903, and nine molecular species in NGC 4414. Then, I proceeded to analyze what was their relationship that they had with the total gas and the dense gas of the molecular cloud. For this, the spectrum was normalized with respect to the ^{13}CO and HCN molecules since each one is related to the total gas and the dense gas respectively. Finally, the abundances of the most relevant detected molecules were calculated assuming that they all have the same excitation temperature (10 K), that is, they were in LTE. These abundances were normalized with respect to the C^{18}O molecule and were compared with “typical” AGNs and Starburst found in the literature.

The conclusions reached with the development of this work were the following:

- This is the first time that most of the molecules have been detected in the three galaxies of my sample. The only lines found in the literature are HCN (1-0), HCO^+ (1-0), and ^{13}CO (1-0) in NGC 4826, and HCN (1-0) and ^{13}CO (1-0) in NGC 2903. However, in literature there is no calculation of its abundances.
- In the study of the intensity of the lines of the spectra, it was found that HCN and HCO^+ are more intense in the Starbursts, while CS is more intense in the AGN. The predominant intensity of ^{13}CO in the spectra is a typical feature of spiral galaxies and its intensity relative to the other lines decreases as the nuclear activity of the galaxy increases. The ratio between ^{13}CO and HNC varies according to the nuclear activity of the galaxies,

when the nuclear activity is low ^{13}CO is higher than HNC , while when the nuclear activity is high HNC tends to be higher than ^{13}CO . These trends found in this work coincide with what is cited in the literature.

- Column densities calculated in this work tend to be at least two orders of magnitude less than those found in the literature. The reason for this difference is probably the low rate of star formation that the galaxies in my sample have. On the other hand, due to the low columnar densities obtained, it could be said that the galaxies have little molecular gas, which would explain the low star formation rate mentioned above.
- Probably, what gives the characteristic to an AGN or Starburst is the environment of the total gas of the molecular cloud since when comparing the normalized columnar density with respect to ^{13}CO and HNC obtained in this work, it was evidenced that in the ratio with HNC the densities between galaxies were approximately constant, while in the ratio with ^{13}CO it was seen that the predominance of certain molecules in AGNs or Starburst.
- **It was found that the environment of NGC 2903 might be similar to M83 which is an example of a galaxy whose starburst is in an intermediate state of evolution, while the environments of NGC 4826 and NGC 4414 might be similar to NGC 1068 which is classified as a Seyfert-2 type galaxy. This means that the galaxies in my sample have a “typical” behavior of galaxies whose nuclear activity is similar.**

5.2 Future Research

To complement the study carried out in this work, it is suggested to carry out the following research:

- As mentioned in section 2.3.2, since the spatial distribution of the molecular gas is not known for any galaxy studied in this work, its antenna temperature was not calibrated by these parameter. For this reason, it is recommended to carry out new observations where this spatial distribution can be calculated, and the proper temperature calibration can be carried out since more precise results would be expected. The type of observations that must be made for this purpose are those of interferometry that can be obtained using Atacama Large Millimeter/submillimeter Array (ALMA) or NOthern Extended Millimeter Array (NOEMA) depending on whether the object of interest is to the south or north of the celestial sphere respectively.
- As mentioned in section 3.1, this work shows for the first time the detection and abundance calculation of each molecule of the three studied galaxies. There is no previous literature that has made this research. For this reason, it is suggested to observe these galaxies again but with another instrument or using another observation technique to confirm the detection of the molecules, especially those that are not common and their transition is complex. Once the detection of this type of molecule has been confirmed, it is suggested to do all the analysis carried out in this work but with this type of molecule.
- As mentioned in section 3.3, the abundances calculation of the molecules was carried out under the assumption that they were in LTE, that is, all transitions occur under the same excitation temperature which for the development of this work was 10K. However, this is a strong assumption and not necessarily true in most

cases where dense molecular clouds are studied. For this reason, a non-LTE study is suggested using LVG type codes or Montecarlo.

Appendix A

Errors Propagation

The errors calculated in this work were obtained by applying the general formula for error propagation⁶²:

If

$$q = q(x, \dots, z), \quad (\text{A.1})$$

then

$$\delta q = \sqrt{\left(\frac{\partial q}{\partial x} \delta x\right)^2 + \dots + \left(\frac{\partial q}{\partial z} \delta z\right)^2}. \quad (\text{A.2})$$

In this way, the error for N_j (Eq. 3.7) is:

$$\delta N_l = \frac{\partial N_l}{\partial I} \delta I, \quad (\text{A.3})$$

where $I = \int T_{mb} dV$, and the error for N_{tot} (Eq. 3.8) is:

$$\delta N_{tot} = \sqrt{\left(\frac{\partial N_{tot}}{\partial N_J} \delta N_J\right)^2 + \left(\frac{\partial N_{tot}}{\partial Z} \delta Z\right)^2}. \quad (\text{A.4})$$

Bibliography

- [1] E. P. Hubble. *Realm of the Nebulae*. 1936.
- [2] R. Buta. *Galaxies: Classification*, page 1666. 2000.
- [3] Frank H. Shu, Fred C. Adams, and Susana Lizano. Star formation in molecular clouds: observation and theory. *Annual Review of Astronomy and Astrophysics*, 25:23–81, January 1987.
- [4] Rebeca Aladro, Sergio Martín, Denise Riquelme, Christian Henkel, Rainer Mauersberger, Jesús Martín-Pintado, Axel Weiss, Charlène Lefèvre, Carsten Kramer, Miguel Requena Torres, and Jairo Armijos. Lambda = 3 mm line survey of nearby active galaxies. *Astronomy Astrophysics*, 579, 04 2015.
- [5] ANGLADA PONS GUILLEM ESTALELLA, ROBERT. *Introducción a la Física del Medio Interestelar*. Publicacions i Edicions de la Universitat de Barcelona.
- [6] James Lochner, Lisa Williamson, and Ethel Fitzhugh. Imagine the universe: The hidden lives of galaxies. 02 2000.
- [7] Rodney Delgado Serrano. *The Evolution of the Hubble Sequence: morpho-kinematics of distant galaxies*. PhD thesis, Observatoire de Paris, 10 2010.
- [8] Roberto G. Abraham and Sidney van den Bergh. The morphological evolution of galaxies. *Science*, 293(5533):1273–1278, 2001.
- [9] Yen-Chen Chen and Chorng-Yuan Hwang. Morphology of seyfert galaxies. *Astrophysics and Space Science*, 362, 07 2017.
- [10] Anil K. Pradhan and Sultana N. Nahar. *Atomic Astrophysics and Spectroscopy*. Cambridge University Press, 2011.
- [11] ESA NASA and the Hubble Heritage (STScI/AURA)-ESA/Hubble Collaboration. Spiral galaxy.
- [12] Michael Joner David Laney (West Mountain Observatory BYU Subaru Telescope (NAOJ), Hubble Legacy Archive. Astronomy picture of the day.

- [13] Gregory A. Shields. A brief history of active galactic nuclei. *Publications of the Astronomical Society of the Pacific*, 111(760):661–678, Jun 1999.
- [14] Jose Sabater Montes. *Nuclear activity and interstellar medium in a sample of isolated galaxies*. PhD thesis, Instituto de Astrofísica de Andalucía-CSIC, 05 2009.
- [15] Bradley M. Peterson. *An Introduction to Active Galactic Nuclei*. 1997.
- [16] F. D. Kahn. Cocoons around early-type stars. *Annual Review of Astronomy and Astrophysics*, 37:149–162, December 1974.
- [17] Christopher McKee and Eve Ostriker. Theory of star formation. *Annual Review of Astronomy and Astrophysics*, 45, 08 2007.
- [18] Ricardo Retes Romero. *Población estelar joven embebida en la nube molecular galáctica asociada a la fuente IRAS 18236-1205*. PhD thesis, Instituto Nacional de Astrofísica, Óptica y Electrónica, 06 2008.
- [19] Antonio Usero. El medio molecular en galaxias con brotes de formación estelar y en galaxias activas. pages 383 – 413, n/d.
- [20] Andrea Silva Bustamante. *Acreción en Núcleos Densos Masivos*. PhD thesis, Universidad de Chile, 2010.
- [21] Dale A. Ostlie Bradley W. Carroll. *An Introduction to Modern Astrophysics*. Cambridge University Press, 2017.
- [22] Eric Herbst and William Klemperer. The Formation and Depletion of Molecules in Dense Interstellar Clouds. *The Astrophysical Journal*, 185:505–534, oct 1973.
- [23] María Mercedes Vazzano. *Estudio multispectral de regiones de formación estelar*. PhD thesis, Universidad Nacional de la Plata, 08 2018.
- [24] J. M. C. Rawlings, S. D. Taylor, and D. A. Williams. A source of extended HCO⁺ emission in young stellar objects. *Monthly Notices of the Royal Astronomical Society*, 313(3):461–468, 04 2000.
- [25] Tomoya Hirota, Satoshi Yamamoto, Hitomi Mikami, and Masatoshi Ohishi. Abundances of HCN and HNC in Dark Cloud Cores. *The Astrophysical Journal*, 503(2):717–728, August 1998.
- [26] R. Meijerink and M. Spaans. Diagnostics of irradiated gas in galaxy nuclei. I. A far-ultraviolet and X-ray dominated region code. *Annual Review of Astronomy and Astrophysics*, 436(2):397–409, June 2005.
- [27] R. Bachiller and M. Pérez Gutiérrez. Shock Chemistry in the Young Bipolar Outflow L1157. *The Astrophysical Journal*, 487(1):L93–L96, September 1997.
- [28] Rodríguez-Fernández, N. J., Tafalla, M., Gueth, F., and Bachiller, R. Hnc enhancement by shocks in the l1157 molecular outflow. *A&A*, 516:A98, 2010.

- [29] S. R. Kulkarni, D. A. Perley, and A. A. Miller. The redshift completeness of local galaxy catalogs. *The Astrophysical Journal*, 860(1):22, Jun 2018.
- [30] H. B. Ann, Mira Seo, and D. K. Ha. A Catalog of Visually Classified Galaxies in the Local ($z \sim 0.01$) Universe. *The Astrophysical Journal Supplement Series*, 217(2):27, April 2015.
- [31] Aaron E. Watkins, J. Christopher Mihos, and Paul Harding. The Red and Featureless Outer Disks of Nearby Spiral Galaxies. *The Astrophysical Journal*, 826(1):59, July 2016.
- [32] M. Krips, R. Neri, S. García-Burillo, S. Martín, F. Combes, J. Graciá-Carpio, and A. Eckart. A Multi-Transition HCN and HCO⁺ Study of 12 Nearby Active Galaxies: Active Galactic Nucleus versus Starburst Environments. *The Astrophysical Journal*, 677(1):262–275, April 2008.
- [33] F. Casoli and M. Gerin. CO in the 'Black Eye' galaxy NGC 4826. *Annual Review of Astronomy and Astrophysics*, 279:L41–L44, November 1993.
- [34] Selcuk Topal. Multiple-line study of molecular gas in spiral galaxy ngc 2903. *Turkish Journal of Physics*, 42:706–720, 12 2018.
- [35] B. Vila-Vilaro, J. Cepa, and A. Zabludoff. The Arizona Radio Observatory Survey of Molecular Gas in Nearby Normal Spiral Galaxies I: The Data. *The Astrophysical Journal Supplement Series*, 218(2):28, June 2015.
- [36] S. Thater, D. Krajnović, M. A. Bourne, M. Cappellari, T. de Zeeuw, E. Emsellem, J. Magorrian, R. M. McDermid, M. Sarzi, and G. van de Ven. A low upper mass limit for the central black hole in the late-type galaxy NGC 4414. *Annual Review of Astronomy and Astrophysics*, 597:A18, January 2017.
- [37] Bradley A. Jacobs, Luca Rizzi, R. Brent Tully, Edward J. Shaya, Dmitry I. Makarov, and Lidia Makarova. The Extragalactic Distance Database: Color-Magnitude Diagrams. *The Astronomical Journal*, 138(2):332–337, August 2009.
- [38] O. Vallejo, J. Braine, and A. Baudry. The stellar mass to light ratio in the isolated spiral NGC 4414. *Annual Review of Astronomy and Astrophysics*, 387:429–440, May 2002.
- [39] Dmitry Makarov, Philippe Prugniel, Nataliya Terekhova, H el ene Courtois, and Isabelle Vauglin. HyperLEDA. III. The catalogue of extragalactic distances. *Annual Review of Astronomy and Astrophysics*, 570:A13, October 2014.
- [40] Volker Heesen, Elias Brinks, Adam K. Leroy, George Heald, Robert Braun, Frank Bigiel, and Rainer Beck. The radio continuum-star formation rate relation in wsrts galaxies. *The Astronomical Journal*, 147(5):103–141, 5 2014.
- [41] Itziar Aretxaga William M. Irvine, Esperanza Carrasco. *The Large Millimeter Telescope: Neighbors Explore the Cosmos*. 2005.

- [42] UMass University. The toltec project. enabling a new view of the obscured universe.
- [43] GTM Alfonso Serrano. Redshift search receiver (rsr).
- [44] J. A. Zavala, M. S. Yun, I. Aretxaga, D. H. Hughes, G. W. Wilson, J. E. Geach, E. Egami, M. A. Gurwell, D. J. Wilner, Ian Smail, A. W. Blain, S. C. Chapman, K. E. K. Coppin, M. Dessauges-Zavadsky, A. C. Edge, A. Montaña, K. Nakajima, T. D. Rawle, D. Sánchez-Argüelles, A. M. Swinbank, T. M. A. Webb, and M. Zeballos. Early Science with the Large Millimeter Telescope: observations of dust continuum and CO emission lines of cluster-lensed submillimetre galaxies at $z=2.0-4.7$. *Monthly Notices of the Royal Astronomical Society*, 452(2):1140–1151, 07 2015.
- [45] A. L. Longinotti, O. Vega, Y. Krongold, I. Aretxaga, M. Yun, V. Chavushyan, C. Feruglio, A. Gómez-Ruiz, A. Montaña, J. León-Tavares, A. Olguín-Iglesias, M. Giroletti, M. Guainazzi, J. Kotilainen, F. Panessa, L. A. Zapata, I. Cruz-Gonzalez, V. M. Patiño-Álvarez, D. Rosa-Gonzalez, A. Carramiñana, L. Carrasco, E. Costantini, D. Dultzin, J. Guichard, I. Puerari, and M. Santos-Lleo. Early Science with the Large Millimeter Telescope: An Energy-driven Wind Revealed by Massive Molecular and Fast X-Ray Outflows in the Seyfert Galaxy IRAS 17020+4544. *The Astrophysical Journal*, 867(1):L11, November 2018.
- [46] B. E. Turner. A Molecular Line Survey of Sagittarius B2 and Orion-KL from 70 to 115 GHz. II. Analysis of the Data. *Astrophysical Journal Supplement Series*, 76:617, June 1991.
- [47] Thomas L. Wilson, Kristen Rohlf, and Susanne Hüttemeister. *Tools of Radio Astronomy*. Springer, 2013.
- [48] Yoshimasa Watanabe, Nami Sakai, Kazuo Sorai, and Satoshi Yamamoto. Spectral line survey toward spiral arm of m51 in the 3 mm and 2 mm bands. *The Astrophysical Journal*, 788, 04 2014.
- [49] Aladro, R., Viti, S., Bayet, E., Riquelme, D., Martín, S., Mauersberger, R., Martín-Pintado, J., Requena-Torres, M. A., Kramer, C., and Weiß, A. A 3 mm molecular line survey of ngc8 - chemical signatures of an agn environment. *A&A*, 549:A39, 2013.
- [50] Taku Nakajima, Shuro Takano, Kotaro Kohno, Nanase Harada, and Eric Herbst. A molecular line survey toward the nearby galaxies ngc1068, ngc253, and ic342 at 3mm with the nobeyama 45 m radio telescope: Impact of an agn on 1 kpc scale molecular abundances. *Publications of the Astronomical Society of Japan*, 70(1), Jan 2018.
- [51] M. A. Frerking, W. D. Langer, and R. W. Wilson. The relationship between carbon monoxide abundance and visual extinction in interstellar clouds. *The Astrophysical Journal*, 262:590–605, November 1982.
- [52] M. Krips, R. Neri, S. García-Burillo, S. Martín, F. Combes, J. Graciá-Carpio, and A. Eckart. A multi-transition HCN and HCO study of 12 nearby active galaxies: Active galactic nucleus versus starburst environments. *The Astrophysical Journal*, 677(1):262–275, apr 2008.
- [53] Jr. Thronson, Harley A., Mark Hereld, Steven Majewski, Matthew Greenhouse, Paul Johnson, Earl Spillar, C. E. Woodward, D. A. Harper, and Bernard J. Rauscher. Near-Infrared Images of NGC 1068: Bar-driven Star Formation and the Circumnuclear Composition. *The Astrophysical Journal*, 343:158, August 1989.

- [54] Richard de Grijs. Star formation timescales in M82. *Astronomy Geophysics*, 42(4):4.12–4.17, 08 2001.
- [55] C. Henkel, H. Asiri, Y. Ao, S. Aalto, A. L. R. Danielson, P. P. Papadopoulos, S. García-Burillo, R. Aladro, C. M. V. Impellizzeri, R. Mauersberger, S. Martín, and N. Harada. Carbon and oxygen isotope ratios in starburst galaxies: New data from NGC 253 and Mrk 231 and their implications. *A&A*, 565:A3, May 2014.
- [56] David S. Meier and Jean L. Turner. Spatially resolved chemistry in nearby galaxies. i. the center of IC 342. *The Astrophysical Journal*, 618(1):259–280, jan 2005.
- [57] S. Lepp and A. Dalgarno. X-ray-induced chemistry of interstellar clouds. *Annual Review of Astronomy and Astrophysics*, 306:L21–L24, February 1996.
- [58] Susanne Aalto. Chemistry in luminous AGN and starburst galaxies. *Astrophysics and Space Science*, 313(1-3):273–278, January 2008.
- [59] Kotaro Kohno, Koichiro Nakanishi, Tomoka Tosaki, Kazuyuki Muraoka, Rie Miura, Hajime Ezawa, and Ryohei Kawabe. Dense gas in normal and active galaxies. *Astrophysics and Space Science*, 313(1-3):279–285, January 2008.
- [60] Edwin A. Bergin, João Alves, Tracy Huard, and Charles J. Lada. N₂h⁺ and c¹⁸o depletion in a cold dark cloud. *The Astrophysical Journal*, 570(2):L101–L104, may 2002.
- [61] Sergio Martín, J. Martín-Pintado, and R. Mauersberger. HNC0 Abundances in Galaxies: Tracing the Evolutionary State of Starbursts. *The Astrophysical Journal*, 694(1):610–617, March 2009.
- [62] J. Reid Mumford. Error propagation reference.

Abbreviations

- ADS** Astrophysics Data System 14
AGN Active Galactic Nucleus iii, 5, 11
ALMA Atacama Large Millimeter/submillimeter Array 50
ARO Arizona Radio Observatory 40, 41
AzTEC Astronomical Thermal Emission Camera 17
- BIMA** Berkeley-Illinois-Maryland Association 41
- CND** Circumnuclear disk 43
- DREAMPY** Data REduction and Analysis Methods in PYthon 19
- FCRAO** Five College Radio Astronomy Observatory 17, 18
FWHM Full width at half maximum 23, 27
- IM** Interstellar Medium 6
INAOE Instituto Nacional de Astrofísica, Óptica y Electrónica 15
IRAM Institut de Radioastronomie Milimétrique 41
- JCMT** James Clerk Maxwell Telescope 18
- LMT** Large Millimeter Telescope iii, 15
LTE Local Thermodynamic Equilibrium iii, 9
- NOEMA** NOrthern Extended Millimeter Array 50
NRAO National Radio Astronomy Observatory 41
- PDR** Photon-dominated region 43
- RSR** Redshift Search Receiver iii, 17, 18
- SB** Starbursts 11

SEQUOIA SEcond QUabbin Optical Imaging Array 17

ULIRG Ultra-luminous infrared galaxy 38

XDR X-ray dominated region 43

YSO Young Stellar Objects 9